Size-dependant behaviour of functionally graded microplates based on the modified strain gradient elasticity theory and isogeometric analysis

Son Thai[a], Huu-Tai Thai[a,*], Thuc P. Vo[b,*], Vipulkumar Ishvarbhai Patel[c]

[a]*School of Engineering and Mathematical Sciences, La Trobe University, Bundoora, VIC 3086, Australia*
[b]*Department of Mechanical and Construction Engineering, Northumbria University, Ellison Place, Newcastle upon Tyne NE1 8ST, UK*
[c]*School of Engineering and Mathematical Sciences, La Trobe University, Bendigo, VIC 3552, Australia*

Abstract

This paper presents a robust numerical model, which takes into account both size-dependent and shear deformation effects, for the bending, buckling and free vibration analyses of functionally graded microplates. The size-dependent effect is captured by using the modified strain gradient elasticity theory with three length scale parameters, whilst the shear deformation effect is accounted by using the third-order shear deformation theory. The rule of mixture is employed to describe the distributions of material phrases through the plate thickness. By using Hamilton's principle, the governing equations are derived and then discretized by employing an Isogeometric Analysis (IGA) approach, where the Non-Uniform Rational B-Splines (NURBS) basis functions are adopted to meet the C^2-continuity requirement. Physical mesh convergence and verification studies are performed to prove the accuracy and reliability of the present model. In addition, parametric studies are also carried out to investigate the size effect in conjunction with the influences of gradient index, shear deformation effect and boundary conditions on the responses of microplates.

Keywords: Size effects, Modified strain gradient elasticity theory, Third-order shear deformation plate theory, Functionally graded materials, Isogeometric Analysis

1. Introduction

In recent years, Functionally Graded Materials (FGMs) known as advanced materials have been broadly investigated in the field of structural mechanics. Being made from a mixture of different phrases of materials with their properties varying continuously through the thickness, Functionally Graded (FG) structures do not have stress concentrations found in laminated composite counterparts. The pioneering work on FGMs was carried out by a group of Japanese material scientists [1, 2]. Typically, a FG structure consists of two material phrases, which are technically called ceramic

*Corresponding author. E-mail: tai.thai@latrobe.edu.au (H.-T. Thai), thuc.vo@northumbria.ac.uk (T.P. Vo)

and metal. The ceramic component is low thermal conductivity and thus has higher temperature-resistant, whereas the metal one is more ductile to prevent thermal stress causing fractures. FGMs have not only used in macro-scale [3–12] but also in nano- and micro-scale applications such as thin films [13, 14], atomic force microscopes (AFMs) [15], micro- and nano-electro-mechanical systems (MEMS and NEMS) [16]. It is worth noting that mirobeams and microplates are the fundamental structures broadly employed in AFM, MEMS and NEMS. Having the small-size features, the behaviour of such structures are considerably affected by size-dependant phenomena, which were verified experimentally.

The size effects were observed in plastic deformation of some metals in the work of Guo et al. [17] and Poole et al. [18]. A considerable size-dependency was observed in the work of Chong and Lam [19] for epoxy and Lam et al. [20] for epoxy polymeric beams. Additionally, a remarkable discrepancy between the experimental and numerical results of microbeams obtained from classical beam theory was reported in the work of McFarland and Colton [21]. Liu at al. [22] carried out a micro-torsion test and they found out that the reduction of wires diameter results in an increase in the torsion strength of thin copper wires. Overall, the aforementioned experimental studies revealed that the classical elasticity theory fails to predict accurately the behaviour of structures at micro-scale. This could be attributed to the presence of material length scale parameters which used to account for size-dependant phenomena. Consequently, there have been a number of theories developed to account for the size effects, in which the length scale paprameters are involved in the constitutive equations. One of the first high-order elasticity theories is classical couple stress theory proposed by Toupin [23], Mindlin and Tiersten [24] and Koiter [25]. It has two material length scale parameters for isotropic elastic materials. The Modified Coupled Stress theory (MCT) proposed by Yang et al. [26] considered a high-order equilibrium equation, which results in a symmetric couple stress tensor. Consequently, only one material length scale parameter associated with rotation gradient involved in the constitutive equations. Another class of high-order elasticity theory were introduced by Mindlin [27], in which the first- and second-order gradients of strains tensor are included in the strain energy expression. Mindlin and Eshel [28] suggested a modified theory which is only first-order gradient of strain tensor along with five additional material length scale parameters applied for isotropic linear elastic materials. Altan and Aifantis [29] developed a simplified version of the high-order elasticity theory, which involves only one material length scale parameter. Based on the theory of Mindlin [27], Fleck and Hutchinson [30–32] introduced a new theory called the strain gradient theory. The Modified Strain gradient elasticity Theory (MST) was proposed by Lam et al. [20] by modifying the classical strain gradient theory of Mindlin [27] and Mindlin and Eshel [28] to establish a new set of

high-order metrics, where the number of additional length scale parameters was reduced from five to three. Moreover, the MST can be reduced to MCT if two of the three material length scale parameters regarding to dilatation gradient and deviatoric stretch gradient are taken to be zero. In order to analyse the structural behaviour micro-structures, literature reveals that the MCT and MST are widely used. Comparing to the former, the latter theory is more general since it covers dilatation and deviatoric stretch gradient tensors in addition to rotation gradient tensor and classical strain tensor as in the MCT.

The MST has been employed to analyse the size-dependent behaviour of microbeams and microplates. Kong et al. [33] and Wang et al. [34] studied the static and dynamic behaviour of small scale beams in accordance with Euler-Bernoulli beam and Timoshenko beam theories. Akgöz and Civalek [35] investigated the buckling response of microbeams. The strain gradient Euler-Bernoulli and Timoshenko beam theories were also developed by Kahrobaiyan et al. [36] and Zhang et al. [37], respectively. Li et al. [38] proposed a size-dependant bilayered Bernoulli-Euler beam model and addressed the locations of neutral and zero-stress axes. Linear and nonlinear vibrations of FG Timoshenko microbeams were carried out by Ansari et al. [39]. Based on Timoshenko beam theory, Shenas et al. [40] conducted vibration analysis of FG microbeam carrying microparticles in the thermal environment. The static bending, instability and free vibration analyses of simply supported miroplates based on Kirchhoff assumptions were studied by Wang et al. [41]. They pointed out that the size effects are dismissed if the plate thickness is greater than the material length scale parameter about 15 times. Ashoori Movassagh and Mahmoodi [42] employed the extended Kantorovich method to derive approximate closed form solutions for bending behaviour of rectangular Kirchhoff microplates with simply supported and clamped boundary conditions. The results of their work revealed that the material length scale parameter associated with the dilatation gradient has the most influence on bending response of the microplates, while the least effect is found for the parameter corresponded to stretch deviatoric gradient. Sahmani and Ansari [43] used high-order shear deformation plate theory to predict the response of FG microplates with simply supported boundary conditions. Analytical solutions for the bending problems of bi-layered Kirchhoff microplate was derived by Li et al. [44]. Ansari et al. [45] also developed a Mindlin plate model to investigate the behaviour of FG circular and annular microplates based on the MST. By using the refined plate theory, Zhang et al. [46, 47] presented studies on the behaviour of rectangular FG microplates resting on elastic foundation and circular/annular FG microplates. The thermoelastic damping of FG microplates was also investigated by Emami and Alibeigloo [48]. Study on the free vibration responses of FG quadrilateral microplates in thermal environment based on Mindlin plate model was conducted by Shenas and

Malekzadeh [49]. Overall, those investigations pointed out a considerable size-dependant behaviour of microbeams and microplates, especially when thickness of the structures is on the same order of the material length scale parameter. In addition, it is seen that most of the aforementioned studies were carried out based on analytical approaches, which were limited to certain types of boundary conditions, loading patterns and geometries. Recently, Mirsalehi et al. [50] employed a finite strip method to study the buckling and free vibration of FG thin square microplates. However, their work is only applicable for thin FG microplates due to the adoption of Kirchhoff theory.

The IGA approach was firstly introduced by Hughes et al. [51] in 2005. Since then, it quickly becomes a hit in many fields of computational mechanics, where its efficiency compared to traditional Finite Element Analysis (FEA) was proven [52]. The fundamental concept of the IGA is to bridge the gap between the methods for analysis and conventional computer-aided design tools using NURBS basis functions. Therefore, the time taken from preliminary designs to analysis progress is reduced considerably while exact geometries of the modelled objects are preserved. The compelling advantages of the IGA have been proved through a large number of publications for plate problems [53–75]. Having distinguished features, the NURBS basis functions are capable of providing a smooth and high continuity interpolation, which allows to construct the elements in a straightforward manner. The shear locking phenomenon can also be reduced with higher order-degree basis functions [62]. Furthermore, circular and annular plates as well as plates with complicated cutouts were successfully modelled with exact geometry by using IGA techniques [5, 43, 52, 54–57, 57–59, 61, 63–65, 71, 73–75].

Although the IGA approach has been successfully applied to investigate the size-dependant behaviour of FG plates based on the non-local elasticity theory [76] and MCT [77, 78], no effort has been devoted to extend this efficient approach to FG microplates based on the MST. The main objective of this study is therefore to develop a robust numerical model used to investigate the bending, free vibration and buckling responses of FG microplates in accordance with the MCT. The third-order shear deformation theory of Reddy [79] is adopted to takes into account the shear deformation effect, while the effect of material variations through the plate thickness is considered using the rule of mixture. Hamilton's principle is used to construct the weak form equations. Then, the NURBS basis functions are employed to interpolate the displacement field and the geometries of rectangular and circular microplates. Physical mesh convergence and verification studied are also carried out to show the reliability and the accuracy. Furthermore, parametric studies are also carried out to investigate the size effect in conjunction with the influences of gradient index, shear deformation effect and boundary conditions on the responses of microplates.

2. Theoretical formulation

2.1. Modified strain gradient elasticity theory

Lam et al. [20] modified the strain gradient theory by decomposing the second-order deformation gradients into three parts (the dilatation gradient vector ζ_i, the deviatoric stretch gradient tensor $\eta^{(1)}_{ijk}$ and the rotation gradient tensor χ^s_{ij} using three different internal length scales. The second-order deformation metrics are mutually independent and only the dilatation scalar and the dilatation gradient vector depend on volumetric deformation. Dilatation gradient is 1st-order tensor, which implies the dilatations in each direction. The deviatoric stretch gradient is 3rd-order tensor, which represents the stretching effect. Rotation gradient is 2nd-order tensor, which expresses the rotation effect. Lam et al. [20] also derived the corresponding work-conjugate stress metrics as the basic strain and stress measures of the strain gradient theory. Hence, the virtual strain energy is given as a summation of four components as

$$\delta U = \int_V \left(\sigma_{ij}\delta\varepsilon_{ij} + p_i\delta\varsigma_i + \tau^{(1)}_{ijk}\delta\eta^{(1)}_{ijk} + m^s_{ij}\delta\chi^s_{ij} \right) dV \tag{1}$$

where the strain tensor ε_{ij} and strain gradient tensors ζ_i, $\eta^{(1)}_{ijk}$, and χ^s_{ij} are expressed as follows

$$\varepsilon_{ij} = \frac{1}{2}\left(\frac{\partial u_i}{\partial x_j} + \frac{\partial u_j}{\partial x_i} \right) \tag{2a}$$

$$\varsigma_i = \frac{\partial \varepsilon_{mm}}{\partial x_i} \tag{2b}$$

$$\begin{aligned} \eta^{(1)}_{ijk} = {} & \frac{1}{3}\left(\frac{\partial \varepsilon_{jk}}{\partial x_i} + \frac{\partial \varepsilon_{ki}}{\partial x_j} + \frac{\partial \varepsilon_{ij}}{\partial x_k} \right) \\ & - \frac{1}{15}\left[\delta_{ij}\left(\frac{\partial \varepsilon_{mm}}{\partial x_k} + 2\frac{\partial \varepsilon_{mk}}{\partial x_m} \right) + \delta_{jk}\left(\frac{\partial \varepsilon_{mm}}{\partial x_i} + 2\frac{\partial \varepsilon_{mi}}{\partial x_m} \right) + \delta_{ki}\left(\frac{\partial \varepsilon_{mm}}{\partial x_j} + 2\frac{\partial \varepsilon_{mj}}{\partial x_m} \right) \right] \end{aligned} \tag{2c}$$

$$\chi^s_{ij} = \frac{1}{4}\left(e_{imn}\frac{\partial^2 u_n}{\partial x^2_{mj}} + e_{jmn}\frac{\partial^2 u_n}{\partial x^2_{mi}} \right) \tag{2d}$$

in which u_i are the components of displacement vector, δ_{ij} is the Kronocker delta and e_{ijk} is the permutation symbol.

The classical stress tensor (σ_{ij}) and high-order stresses $(p_i, \tau^{(1)}_{ijk}$, and $m^s_{ij})$ associated with gradient tensors are given by the following constitutive relations

$$\sigma_{ij} = 2\mu\varepsilon_{ij} + \lambda\varepsilon_{kk}\delta_{ij} \tag{3a}$$

$$p_i = 2\mu l_0^2 \varsigma_i \tag{3b}$$

$$\tau^{(1)}_{ijk} = 2\mu l_1^2 \eta^{(1)}_{ijk} \tag{3c}$$

$$m_{ij}^{s} = 2\mu l_2^2 \chi_{ij}^{s} \tag{3d}$$

where l_0, l_1 and l_2 are the additional material length scale parameters corresponding to the dilatation gradient tensor, deviatoric stretch gradient tensor and symmetric rotation gradient tensor, respectively. λ and μ are the the Lamé constants and are given by

$$\lambda = \frac{\nu E(z)}{[1+\nu(z)]\,[1-2\nu(z)]};\;\; \mu = \frac{E(z)}{2\,[1+\nu(z)]} \tag{4}$$

2.2. Material properties of FGM

Consider rectangular and circular FG microplates whose dimensions are depicted in Fig. 1. The x and y coordinates are located in the midplane Ω of the plate, and the z-axis is normal to the midplane. According to the rule of mixture, material properties vary through the thickness h of the FG microplates follow the law stated as

$$P\,(z) = (P_c - P_m)\,V + P_m \tag{5a}$$

where V is the volume fraction and defined as

$$V = \left(\frac{z}{h} + \frac{1}{2}\right)^{n} \tag{5b}$$

in which $P(z)$ denotes a generic material property such as Young's modulus $E(z)$, Possion's ratio $\nu(z)$, density $\rho(z)$. P_c and P_m are the material properties of ceramic and metal component, and n is the material gradient index used to indicate the profiles of material phrases through the thickness. When n = 0, a full ceramic plate is obtained, whereas a full metal one is observed by setting n = ∞.

2.3. Third-order shear deformation theory

Based on the third-order shear deformation theory of Reddy [79], the displacement field is expressed as follows

$$\begin{aligned} u_1 &= u + f\,(z)\,\theta_x - g\,(z)\,\tfrac{\partial w}{\partial x} \\ u_2 &= v + f\,(z)\,\theta_y - g\,(z)\,\tfrac{\partial w}{\partial y} \\ u_3 &= w \end{aligned} \tag{6}$$

where (u, v, w) are the displacements along the x, y, z coordinate directions, respectively, (θ_x, θ_y) are the angular displacements in the x and y direction, and

$$f\,(z) = z - \frac{4z^3}{3h^2};\;\; g\,(z) = \frac{4z^3}{3h^2} \tag{7}$$

Substituting Eq. (6) into Eq. (2), the strain-displacement relations of strain tensor ε_{ij} and strain gradient tensors ζ_i, $\eta_{ijk}^{(1)}$, χ_{ij} are obtained.

The strain tensor ε_{ij} is given by

$$\boldsymbol{\varepsilon} = \boldsymbol{\varepsilon}_0 + f(z)\,\boldsymbol{\varepsilon}_1 + g(z)\,\boldsymbol{\varepsilon}_2 \tag{8a}$$

$$\boldsymbol{\gamma} = f'(z)\,\boldsymbol{\gamma}_1 + (1 - g'(z))\,\boldsymbol{\gamma}_2 \tag{8b}$$

where

$$\boldsymbol{\varepsilon} = \begin{Bmatrix} \varepsilon_{xx} \\ \varepsilon_{yy} \\ \gamma_{xy} \end{Bmatrix};\ \boldsymbol{\varepsilon}_0 = \begin{Bmatrix} \frac{\partial u}{\partial x} \\ \frac{\partial v}{\partial y} \\ \frac{\partial u}{\partial y} + \frac{\partial v}{\partial x} \end{Bmatrix};\boldsymbol{\varepsilon}_1 = \begin{Bmatrix} \frac{\partial \theta_x}{\partial x} \\ \frac{\partial \theta_y}{\partial y} \\ \frac{\partial \theta_x}{\partial y} + \frac{\partial \theta_y}{\partial x} \end{Bmatrix};\boldsymbol{\varepsilon}_2 = \begin{Bmatrix} -\frac{\partial^2 w}{\partial x^2} \\ -\frac{\partial^2 w}{\partial y^2} \\ -2\frac{\partial^2 w}{\partial x \partial y} \end{Bmatrix} \tag{9a}$$

$$\boldsymbol{\gamma} = \begin{Bmatrix} \gamma_{xz} \\ \gamma_{yz} \end{Bmatrix};\ \boldsymbol{\gamma}_1 = \begin{Bmatrix} \theta_x \\ \theta_y \end{Bmatrix};\boldsymbol{\gamma}_2 = \begin{Bmatrix} \frac{\partial w}{\partial x} \\ \frac{\partial w}{\partial y} \end{Bmatrix} \tag{9b}$$

The dilatation gradient tensor ζ_i is expressed by

$$\boldsymbol{\varsigma} = \boldsymbol{\varsigma}_0 + f(z)\,\boldsymbol{\varsigma}_1 + g(z)\,\boldsymbol{\varsigma}_2 \tag{10a}$$

$$\varsigma_z = f'(z)\,\varsigma_3 + g'(z)\,\varsigma_4 \tag{10b}$$

where

$$\boldsymbol{\varsigma} = \begin{Bmatrix} \varsigma_x \\ \varsigma_y \end{Bmatrix};\boldsymbol{\varsigma}_0 = \begin{Bmatrix} \frac{\partial^2 u}{\partial x^2} + \frac{\partial^2 v}{\partial x \partial y} \\ \frac{\partial^2 u}{\partial x \partial y} + \frac{\partial^2 v}{\partial y^2} \end{Bmatrix};\boldsymbol{\varsigma}_1 = \begin{Bmatrix} \frac{\partial^2 \theta_x}{\partial x^2} + \frac{\partial^2 \theta_y}{\partial x \partial y} \\ \frac{\partial^2 \theta_x}{\partial x \partial y} + \frac{\partial^2 \theta_y}{\partial y^2} \end{Bmatrix};\boldsymbol{\varsigma}_2 = \begin{Bmatrix} -\frac{\partial^3 w}{\partial x^3} - \frac{\partial^3 w}{\partial x \partial y^2} \\ -\frac{\partial^3 w}{\partial x^2 \partial y} - \frac{\partial^3 w}{\partial y^3} \end{Bmatrix} \tag{11a}$$

$$\varsigma_3 = \frac{\partial \theta_x}{\partial x} + \frac{\partial \theta_y}{\partial y};\varsigma_4 = -\frac{\partial^2 w}{\partial x^2} - \frac{\partial^2 w}{\partial y^2} \tag{11b}$$

The deviatoric stretch gradient tensor $\eta^{(1)}_{ijk}$ is defined as

$$\boldsymbol{\eta} = \boldsymbol{\eta}_0 + f''(z)\,\boldsymbol{\eta}_1 + f'(z)\,\boldsymbol{\eta}_2 + f(z)\,\boldsymbol{\eta}_3 + g''(z)\,\boldsymbol{\eta}_4 + g'(z)\,\boldsymbol{\eta}_5 + g(z)\,\boldsymbol{\eta}_6 \tag{12}$$

where

$$\boldsymbol{\eta} = \begin{Bmatrix} \eta^{(1)}_{xxx} \\ \eta^{(1)}_{yyy} \\ \eta^{(1)}_{zzz} \\ \eta^{(1)}_{xxy} \\ \eta^{(1)}_{xxz} \\ \eta^{(1)}_{xyy} \\ \eta^{(1)}_{xyz} \\ \eta^{(1)}_{xzz} \\ \eta^{(1)}_{yyz} \\ \eta^{(1)}_{yzz} \end{Bmatrix};\boldsymbol{\eta}_0 = \begin{Bmatrix} \frac{2}{5}\frac{\partial^2 u}{\partial x^2} - \frac{1}{5}\frac{\partial^2 u}{\partial y^2} - \frac{2}{5}\frac{\partial^2 v}{\partial x \partial y} \\ -\frac{2}{5}\frac{\partial^2 u}{\partial x \partial y} + \frac{2}{5}\frac{\partial^2 v}{\partial y^2} - \frac{1}{5}\frac{\partial^2 v}{\partial x^2} \\ -\frac{1}{5}\frac{\partial^2 w}{\partial x^2} - \frac{1}{5}\frac{\partial^2 w}{\partial y^2} \\ \frac{8}{15}\frac{\partial^2 u}{\partial x \partial y} + \frac{4}{15}\frac{\partial^2 v}{\partial x^2} - \frac{1}{5}\frac{\partial^2 v}{\partial y^2} \\ \frac{4}{15}\frac{\partial^2 w}{\partial x^2} - \frac{1}{15}\frac{\partial^2 w}{\partial y^2} \\ \frac{4}{15}\frac{\partial^2 u}{\partial y^2} - \frac{1}{5}\frac{\partial^2 u}{\partial x^2} + \frac{8}{15}\frac{\partial^2 v}{\partial x \partial y} \\ \frac{1}{3}\frac{\partial^2 w}{\partial x \partial y} \\ -\frac{1}{5}\frac{\partial^2 u}{\partial x^2} - \frac{1}{15}\frac{\partial^2 u}{\partial y^2} - \frac{2}{15}\frac{\partial^2 v}{\partial x \partial y} \\ \frac{4}{15}\frac{\partial^2 w}{\partial y^2} - \frac{1}{15}\frac{\partial^2 w}{\partial x^2} \\ -\frac{2}{15}\frac{\partial^2 u}{\partial x \partial y} - \frac{1}{15}\frac{\partial^2 v}{\partial x^2} - \frac{1}{5}\frac{\partial^2 v}{\partial y^2} \end{Bmatrix};\boldsymbol{\eta}_1 = \begin{Bmatrix} -\frac{1}{5}\theta_x \\ -\frac{1}{5}\theta_y \\ 0 \\ -\frac{1}{15}\theta_y \\ 0 \\ -\frac{1}{15}\theta_x \\ 0 \\ \frac{4}{15}\theta_x \\ 0 \\ \frac{4}{15}\theta_y \end{Bmatrix} \tag{13a}$$

$$\boldsymbol{\eta}_2 = \begin{Bmatrix} 0 \\ 0 \\ -\frac{2}{5}\frac{\partial \theta_x}{\partial x} - \frac{2}{5}\frac{\partial \theta_y}{\partial y} \\ 0 \\ \frac{8}{15}\frac{\partial \theta_x}{\partial x} - \frac{2}{15}\frac{\partial \theta_y}{\partial y} \\ 0 \\ \frac{1}{3}\frac{\partial \theta_x}{\partial y} + \frac{1}{3}\frac{\partial \theta_y}{\partial x} \\ 0 \\ -\frac{2}{15}\frac{\partial \theta_x}{\partial x} + \frac{8}{15}\frac{\partial \theta_y}{\partial y} \\ 0 \end{Bmatrix}; \boldsymbol{\eta}_3 = \begin{Bmatrix} \frac{2}{5}\frac{\partial^2 \theta_x}{\partial x^2} - \frac{1}{5}\frac{\partial^2 \theta_x}{\partial y^2} - \frac{2}{5}\frac{\partial^2 \theta_y}{\partial x \partial y} \\ -\frac{2}{5}\frac{\partial^2 \theta_x}{\partial x \partial y} - \frac{1}{5}\frac{\partial^2 \theta_y}{\partial x^2} + \frac{2}{5}\frac{\partial^2 \theta_y}{\partial y^2} \\ 0 \\ \frac{8}{15}\frac{\partial^2 \theta_x}{\partial x \partial y} + \frac{4}{15}\frac{\partial^2 \theta_y}{\partial x^2} - \frac{1}{5}\frac{\partial^2 \theta_y}{\partial y^2} \\ 0 \\ -\frac{1}{5}\frac{\partial^2 \theta_x}{\partial x^2} + \frac{4}{15}\frac{\partial^2 \theta_x}{\partial y^2} + \frac{8}{15}\frac{\partial^2 \theta_y}{\partial x \partial y} \\ 0 \\ -\frac{1}{5}\frac{\partial^2 \theta_x}{\partial x^2} - \frac{1}{15}\frac{\partial^2 \theta_x}{\partial y^2} - \frac{2}{15}\frac{\partial^2 \theta_y}{\partial x \partial y} \\ 0 \\ -\frac{2}{15}\frac{\partial^2 \theta_x}{\partial x \partial y} - \frac{1}{15}\frac{\partial^2 \theta_y}{\partial x^2} - \frac{1}{5}\frac{\partial^2 \theta_y}{\partial y^2} \end{Bmatrix}; \boldsymbol{\eta}_4 = \begin{Bmatrix} \frac{1}{5}\frac{\partial w}{\partial x} \\ \frac{1}{5}\frac{\partial w}{\partial y} \\ 0 \\ \frac{1}{15}\frac{\partial w}{\partial y} \\ 0 \\ \frac{1}{15}\frac{\partial w}{\partial x} \\ 0 \\ -\frac{4}{15}\frac{\partial w}{\partial x} \\ 0 \\ -\frac{4}{15}\frac{\partial w}{\partial y} \end{Bmatrix} \tag{13b}$$

$$\boldsymbol{\eta}_5 = \begin{Bmatrix} 0 \\ 0 \\ \frac{2}{5}\frac{\partial^2 w}{\partial x^2} + \frac{2}{5}\frac{\partial^2 w}{\partial y^2} \\ 0 \\ -\frac{8}{15}\frac{\partial^2 w}{\partial x^2} + \frac{2}{15}\frac{\partial^2 w}{\partial y^2} \\ 0 \\ -\frac{1}{2}\frac{\partial^2 w}{\partial x \partial y} \\ 0 \\ \frac{2}{15}\frac{\partial^2 w}{\partial x^2} - \frac{8}{15}\frac{\partial^2 w}{\partial y^2} \\ 0 \end{Bmatrix}; \boldsymbol{\eta}_6 = \begin{Bmatrix} -\frac{2}{5}\frac{\partial^3 w}{\partial x^3} + \frac{3}{5}\frac{\partial^3 w}{\partial x \partial y^2} \\ -\frac{2}{5}\frac{\partial^3 w}{\partial y^3} + \frac{3}{5}\frac{\partial^3 w}{\partial x^2 \partial y} \\ 0 \\ -\frac{4}{5}\frac{\partial^3 w}{\partial x^2 \partial y} + \frac{1}{5}\frac{\partial^3 w}{\partial y^3} \\ 0 \\ \frac{1}{5}\frac{\partial^3 w}{\partial x^3} - \frac{4}{5}\frac{\partial^3 w}{\partial x \partial y^2} \\ 0 \\ \frac{1}{5}\frac{\partial^3 w}{\partial x^3} + \frac{1}{5}\frac{\partial^3 w}{\partial x \partial y^2} \\ 0 \\ \frac{1}{5}\frac{\partial^3 w}{\partial x^2 \partial y} + \frac{1}{5}\frac{\partial^3 w}{\partial y^3} \end{Bmatrix} \tag{13c}$$

The symmetric part of rotation gradient tensor $\boldsymbol{\chi}$ is given by

$$\boldsymbol{\chi} = \boldsymbol{\chi}_0 + f''(z)\,\boldsymbol{\chi}_1 + f'(z)\,\boldsymbol{\chi}_2 + f(z)\,\boldsymbol{\chi}_3 + g''(z)\,\boldsymbol{\chi}_4 + g'(z)\,\boldsymbol{\chi}_5 \tag{14}$$

where

$$\boldsymbol{\chi} = \begin{Bmatrix} \chi^s_{xx} \\ \chi^s_{yy} \\ \chi^s_{xy} \\ \chi^s_{zz} \\ \chi^s_{xz} \\ \chi^s_{yz} \end{Bmatrix}; \boldsymbol{\chi}_0 = \begin{Bmatrix} \frac{1}{2}\frac{\partial^2 w}{\partial x \partial y} \\ -\frac{1}{2}\frac{\partial^2 w}{\partial x \partial y} \\ \frac{1}{4}\frac{\partial^2 w}{\partial y^2} - \frac{1}{4}\frac{\partial^2 w}{\partial x^2} \\ 0 \\ -\frac{1}{4}\frac{\partial^2 u}{\partial x \partial y} + \frac{1}{4}\frac{\partial^2 v}{\partial x^2} \\ \frac{1}{4}\frac{\partial^2 v}{\partial x \partial y} - \frac{1}{4}\frac{\partial^2 u}{\partial y^2} \end{Bmatrix}; \boldsymbol{\chi}_1 = \begin{Bmatrix} 0 \\ 0 \\ 0 \\ 0 \\ -\frac{1}{4}\theta_y \\ \frac{1}{4}\theta_x \end{Bmatrix}; \boldsymbol{\chi}_2 = \begin{Bmatrix} -\frac{1}{2}\frac{\partial \theta_y}{\partial x} \\ \frac{1}{2}\frac{\partial \theta_x}{\partial y} \\ \frac{1}{4}\frac{\partial \theta_x}{\partial x} - \frac{1}{4}\frac{\partial \theta_y}{\partial y} \\ -\frac{1}{2}\frac{\partial \theta_x}{\partial y} + \frac{1}{2}\frac{\partial \theta_y}{\partial x} \\ 0 \\ 0 \end{Bmatrix} \tag{15a}$$

$$\boldsymbol{\chi}_3=\left\{\begin{array}{c}0\\0\\0\\0\\-\frac{1}{4}\frac{\partial^2\theta_x}{\partial x\partial y}+\frac{1}{4}\frac{\partial^2\theta_y}{\partial x^2}\\-\frac{1}{4}\frac{\partial^2\theta_x}{\partial y^2}+\frac{1}{4}\frac{\partial^2\theta_y}{\partial x\partial y}\end{array}\right\};\boldsymbol{\chi}_4=\left\{\begin{array}{c}0\\0\\0\\0\\\frac{1}{4}\frac{\partial w}{\partial y}\\-\frac{1}{4}\frac{\partial w}{\partial x}\end{array}\right\};\boldsymbol{\chi}_5=\left\{\begin{array}{c}\frac{1}{2}\frac{\partial^2 w}{\partial x\partial y}\\-\frac{1}{2}\frac{\partial^2 w}{\partial x\partial y}\\\frac{1}{4}\frac{\partial^2 w}{\partial y^2}-\frac{1}{4}\frac{\partial^2 w}{\partial x^2}\\0\\0\\0\end{array}\right\} \tag{15b}$$

The prime denotes the derivative with respect to z. Although the transverse normal stress σ_{zz} is dismissed as assumed in the plate theory, it is seen that other transverse normal high-order stresses are not zero at all. The stress resultants corresponding to classical stress and high-order stresses are given as follows

$$\left(N^{\varepsilon}_{\alpha\beta},M^{\varepsilon}_{\alpha\beta},L^{\varepsilon}_{\alpha\beta}\right)=\int_{-h/2}^{h/2}\sigma_{\alpha\beta}\left(1,f\left(z\right),g\left(z\right)\right)dz\ ;\ \left(T^{\varepsilon}_{\alpha z},U^{\varepsilon}_{\alpha z}\right)=\int_{-h/2}^{h/2}\sigma_{\alpha z}\left(f'\left(z\right),1-g'\left(z\right)\right)dz \tag{16a}$$

$$\left(N^{\varsigma}_{\alpha},M^{\varsigma}_{\alpha},L^{\varsigma}_{\alpha}\right)=\int_{-h/2}^{h/2}p_{\alpha}\left(1,f\left(z\right),g\left(z\right)\right)dz\,;\ \left(T^{\varsigma}_{z},U^{\varsigma}_{z}\right)=\int_{-h/2}^{h/2}p_{z}\left(f'\left(z\right),g'\left(z\right)\right)dz \tag{16b}$$

$$\left(N^{\eta}_{ijk},M^{\eta}_{ijk},L^{\eta}_{ijk},T^{\eta}_{ijk},S^{\eta}_{ijk},U^{\eta}_{ijk},R^{\eta}_{ijk}\right)=\int_{-h/2}^{h/2}\tau^{(1)}_{ijk}\left(1,f''\left(z\right),f'\left(z\right),f\left(z\right),g''\left(z\right),g'\left(z\right),g\left(z\right)\right)dz \tag{16c}$$

$$\left(N^{\chi}_{ij},M^{\chi}_{ij},L^{\chi}_{ij},T^{\chi}_{ij},S^{\chi}_{ij},U^{\chi}_{ij}\right)=\int_{-h/2}^{h/2}m^{s}_{ij}\left(1,f''\left(z\right),f'\left(z\right),f\left(z\right),g''\left(z\right),g'\left(z\right)\right)dz \tag{16d}$$

where Greek subscripts α and β represent x and y in turns. Next, substituting Eq. (3) into Eq. (16), the stress resultants of classical stress and high-order stresses can be rewritten as

$$\hat{\boldsymbol{\sigma}}=\left\{\begin{array}{c}\mathbf{N}^{\varepsilon}\\\mathbf{M}^{\varepsilon}\\\mathbf{L}^{\varepsilon}\\\mathbf{T}^{\varepsilon}\\\mathbf{U}^{\varepsilon}\end{array}\right\}=\left[\begin{array}{ccccc}\mathbf{A}^{\varepsilon}&\mathbf{P}^{\varepsilon}&\mathbf{C}^{\varepsilon}&\mathbf{0}&\mathbf{0}\\\mathbf{P}^{\varepsilon}&\mathbf{H}^{\varepsilon}&\mathbf{F}^{\varepsilon}&\mathbf{0}&\mathbf{0}\\\mathbf{C}^{\varepsilon}&\mathbf{F}^{\varepsilon}&\mathbf{G}^{\varepsilon}&\mathbf{0}&\mathbf{0}\\\mathbf{0}&\mathbf{0}&\mathbf{0}&\bar{\mathbf{A}}^{\varepsilon}&\bar{\mathbf{P}}^{\varepsilon}\\\mathbf{0}&\mathbf{0}&\mathbf{0}&\bar{\mathbf{P}}^{\varepsilon}&\bar{\mathbf{C}}^{\varepsilon}\end{array}\right]\left\{\begin{array}{c}\boldsymbol{\varepsilon}_0\\\boldsymbol{\varepsilon}_1\\\boldsymbol{\varepsilon}_2\\\boldsymbol{\gamma}_1\\\boldsymbol{\gamma}_2\end{array}\right\}=\hat{\mathbf{D}}_{\varepsilon}\hat{\boldsymbol{\varepsilon}} \tag{17a}$$

$$\hat{\mathbf{p}}=\left\{\begin{array}{c}\mathbf{N}^{\varepsilon}\\\mathbf{M}^{\varepsilon}\\\mathbf{L}^{\varepsilon}\\\mathbf{T}^{\varepsilon}\\\mathbf{U}^{\varepsilon}\end{array}\right\}=\left[\begin{array}{ccccc}A^{\varsigma}&P^{\varsigma}&C^{\varsigma}&0&0\\P^{\varsigma}&H^{\varsigma}&F^{\varsigma}&0&0\\C^{\varsigma}&F^{\varsigma}&G^{\varsigma}&0&0\\0&0&0&\bar{A}^{\varsigma}&\bar{P}^{\varsigma}\\0&0&0&\bar{P}^{\varsigma}&\bar{C}^{\varsigma}\end{array}\right]\left\{\begin{array}{c}\boldsymbol{\varsigma}_0\\\boldsymbol{\varsigma}_1\\\boldsymbol{\varsigma}_2\\\boldsymbol{\varsigma}_3\\\boldsymbol{\varsigma}_4\end{array}\right\}=\hat{\mathbf{D}}_{\varsigma}\hat{\boldsymbol{\varsigma}} \tag{17b}$$

$$\hat{\boldsymbol{\tau}}=\left\{\begin{array}{c}\mathbf{N}^{\eta}\\ \mathbf{M}^{\eta}\\ \mathbf{L}^{\eta}\\ \mathbf{T}^{\eta}\\ \mathbf{S}^{\eta}\\ \mathbf{U}^{\eta}\\ \mathbf{R}^{\eta}\end{array}\right\}=\left[\begin{array}{ccccccc}A^{\eta} & P^{\eta} & C^{\eta} & Q^{\eta} & \bar{P}^{\eta} & \bar{C}^{\eta} & \bar{Q}^{\eta}\\ P^{\eta} & H^{\eta} & F^{\eta} & Y^{\eta} & \bar{H}^{\eta} & \bar{F}^{\eta} & \bar{Y}^{\eta}\\ C^{\eta} & F^{\eta} & G^{\eta} & Z^{\eta} & \bar{K}^{\eta} & \bar{G}^{\eta} & \bar{Z}^{\eta}\\ Q^{\eta} & Y^{\eta} & Z^{\eta} & W^{\eta} & \bar{I}^{\eta} & \bar{J}^{\eta} & \bar{W}^{\eta}\\ \bar{P}^{\eta} & \bar{H}^{\eta} & \bar{K}^{\eta} & \bar{I}^{\eta} & \widehat{K}^{\eta} & \bar{B}^{\eta} & \bar{O}^{\eta}\\ \bar{C}^{\eta} & \bar{F}^{\eta} & \bar{G}^{\eta} & \bar{J}^{\eta} & \bar{B}^{\eta} & \widehat{I}^{\eta} & \bar{E}^{\eta}\\ \bar{Q}^{\eta} & \bar{Y}^{\eta} & \bar{Z}^{\eta} & \bar{W}^{\eta} & \bar{O}^{\eta} & \bar{E}^{\eta} & \widehat{J}^{\eta}\end{array}\right]\left\{\begin{array}{c}\boldsymbol{\eta}_0\\ \boldsymbol{\eta}_1\\ \boldsymbol{\eta}_2\\ \boldsymbol{\eta}_3\\ \boldsymbol{\eta}_4\\ \boldsymbol{\eta}_5\\ \boldsymbol{\eta}_6\end{array}\right\}=\hat{\mathbf{D}}_{\eta}\hat{\boldsymbol{\eta}} \tag{17c}$$

$$\hat{\mathbf{m}}=\left\{\begin{array}{c}\mathbf{N}^{\chi}\\ \mathbf{M}^{\chi}\\ \mathbf{L}^{\chi}\\ \mathbf{T}^{\chi}\\ \mathbf{S}^{\chi}\\ \mathbf{U}^{\chi}\end{array}\right\}=\left[\begin{array}{cccccc}A^{\chi} & P^{\chi} & C^{\chi} & Q^{\chi} & \bar{P}^{\chi} & \bar{C}^{\chi}\\ P^{\chi} & H^{\chi} & F^{\chi} & Y^{\chi} & \bar{H}^{\chi} & \bar{F}^{\chi}\\ C^{\chi} & F^{\chi} & G^{\chi} & Z^{\chi} & \bar{K}^{\chi} & \bar{G}^{\chi}\\ Q^{\chi} & Y^{\chi} & Z^{\chi} & W^{\chi} & \bar{I}^{\chi} & \bar{J}^{\chi}\\ \bar{P}^{\chi} & \bar{H}^{\chi} & \bar{K}^{\chi} & \bar{I}^{\chi} & \widehat{K}^{\chi} & \bar{B}^{\chi}\\ \bar{C}^{\chi} & \bar{F}^{\chi} & \bar{G} & \bar{J}^{\chi} & \bar{B}^{\chi} & \widehat{I}^{\chi}\end{array}\right]\left\{\begin{array}{c}\boldsymbol{\chi}_0\\ \boldsymbol{\chi}_1\\ \boldsymbol{\chi}_2\\ \boldsymbol{\chi}_3\\ \boldsymbol{\chi}_4\\ \boldsymbol{\chi}_5\end{array}\right\}=\hat{\mathbf{D}}_{\chi}\hat{\boldsymbol{\chi}} \tag{17d}$$

where

$$\left(\mathbf{A}^{\varepsilon},\mathbf{P}^{\varepsilon},\mathbf{C}^{\varepsilon}\right)=\int_{-h/2}^{h/2}\left(1,f\left(z\right),g\left(z\right)\right)\mathbf{Q}_b dz \tag{18a}$$

$$\left(\mathbf{H}^{\varepsilon},\mathbf{F}^{\varepsilon},\mathbf{G}^{\varepsilon}\right)=\int_{-h/2}^{h/2}\left(\left(f\left(z\right)\right)^2,f\left(z\right)g\left(z\right),\left(g\left(z\right)\right)^2\right)\mathbf{Q}_b dz \tag{18b}$$

$$\left(\bar{\mathbf{A}}^{\varepsilon},\bar{\mathbf{P}}^{\varepsilon},\bar{\mathbf{C}}^{\varepsilon}\right)=\int_{-h/2}^{h/2}\left(\left(f'\left(z\right)\right)^2,\left(f'\left(z\right)\right)\left(1-g'\left(z\right)\right),\left(1-g'\left(z\right)\right)^2\right)\mathbf{Q}_s dz \tag{18c}$$

$$\left(A^{\varsigma},P^{\varsigma},C^{\varsigma}\right)=\int_{-h/2}^{h/2}\left(1,f\left(z\right),g\left(z\right)\right)2\mu l_0^2 dz \tag{18d}$$

$$\left(H^{\varsigma},F^{\varsigma},G^{\varsigma}\right)=\int_{-h/2}^{h/2}\left(\left(f\left(z\right)\right)^2,f\left(z\right)g\left(z\right),\left(g\left(z\right)\right)^2\right)2\mu l_0^2 dz \tag{18e}$$

$$\left(A^{\eta},P^{\eta},C^{\eta},Q^{\eta}\right)=\int_{-h/2}^{h/2}\left(1,f''\left(z\right),f'\left(z\right),f\left(z\right)\right)2\mu l_1^2 dz \tag{18f}$$

$$\left(\bar{P}^{\eta},\bar{C}^{\eta},\bar{Q}^{\eta}\right)=\int_{-h/2}^{h/2}\left(g''\left(z\right),g'\left(z\right),g\left(z\right)\right)2\mu l_1^2 dz \tag{18g}$$

$$\left(H^{\eta},F^{\eta},Y^{\eta}\right)=\int_{-h/2}^{h/2}\left(\left(f''\left(z\right)\right)^2,f''\left(z\right)f'\left(z\right),f''\left(z\right)f\left(z\right)\right)2\mu l_1^2 dz \tag{18h}$$

$$\left(\bar{H}^{\eta},\bar{F}^{\eta},\bar{Y}^{\eta}\right)=\int_{-h/2}^{h/2}\left(f''\left(z\right)g''\left(z\right),f''\left(z\right)g'\left(z\right),f''\left(z\right)g\left(z\right)\right)2\mu l_{1}^{2}dz \tag{18i}$$

$$\left(G^{\eta},Z^{\eta},W^{\eta}\right)=\int_{-h/2}^{h/2}\left(\left(f'\left(z\right)\right)^{2},f'\left(z\right)f\left(z\right),\left(f\left(z\right)\right)^{2}\right)2\mu l_{1}^{2}dz \tag{18j}$$

$$\left(\bar{K}^{\eta},\bar{G}^{\eta},\bar{Z}^{\eta}\right)=\int_{-h/2}^{h/2}\left(f'\left(z\right)g''\left(z\right),f'\left(z\right)g'\left(z\right),f'\left(z\right)g\left(z\right)\right)2\mu l_{1}^{2}dz \tag{18k}$$

$$\left(\bar{I}^{\eta},\bar{J}^{\eta},\bar{W}^{\eta}\right)=\int_{-h/2}^{h/2}\left(f\left(z\right)g''\left(z\right),f\left(z\right)g'\left(z\right),f\left(z\right)g\left(z\right)\right)2\mu l_{1}^{2}dz \tag{18l}$$

$$\left(\widehat{K}^{\eta},\bar{B}^{\eta},\bar{O}^{\eta}\right)=\int_{-h/2}^{h/2}\left(\left(g''\left(z\right)\right)^{2},g''\left(z\right)g'\left(z\right),g''\left(z\right)g\left(z\right)\right)2\mu l_{1}^{2}dz \tag{18m}$$

$$\left(\widehat{I}^{\eta},\bar{E}^{\eta},\widehat{J}^{\eta}\right)=\int_{-h/2}^{h/2}\left(\left(g'\left(z\right)\right)^{2},g'\left(z\right)g\left(z\right),\left(g\left(z\right)\right)^{2}\right)2\mu l_{1}^{2}dz \tag{18n}$$

$$\left(A^{\chi},P^{\chi},C^{\chi},Q^{\chi}\right)=\int_{-h/2}^{h/2}\left(1,f''\left(z\right),f'\left(z\right),f\left(z\right)\right)2\mu l_{2}^{2}dz \tag{18o}$$

$$\left(\bar{P}^{\chi},\bar{C}^{\chi}\right)=\int_{-h/2}^{h/2}\left(g''\left(z\right),g'\left(z\right)\right)2\mu l_{2}^{2}dz \tag{18p}$$

$$\left(H^{\chi},F^{\chi},Y^{\chi}\right)=\int_{-h/2}^{h/2}\left(\left(f''\left(z\right)\right)^{2},f''\left(z\right)f'\left(z\right),f''\left(z\right)f\left(z\right)\right)2\mu l_{2}^{2}dz \tag{18q}$$

$$\left(\bar{H}^{\chi},\bar{F}^{\chi}\right)=\int_{-h/2}^{h/2}\left(f''\left(z\right)g''\left(z\right),f''\left(z\right)g'\left(z\right)\right)2\mu l_{2}^{2}dz \tag{18r}$$

$$\left(G^{\chi},Z^{\chi},W^{\chi}\right)=\int_{-h/2}^{h/2}\left(\left(f'\left(z\right)\right)^{2},f'\left(z\right)f\left(z\right),\left(f\left(z\right)\right)^{2}\right)2\mu l_{2}^{2}dz \tag{18s}$$

$$\left(\bar{K}^{\chi},\bar{G}^{\chi}\right)=\int_{-h/2}^{h/2}\left(f'\left(z\right)g''\left(z\right),f'\left(z\right)g'\left(z\right)\right)2\mu l_{2}^{2}dz \tag{18t}$$

$$\left(\bar{I}_{ij}^{\eta},\bar{J}_{ij}^{\eta}\right)=\int_{-h/2}^{h/2}\left(f\left(z\right)g''\left(z\right),f\left(z\right)g'\left(z\right)\right)2\mu l_{1}^{2}dz \tag{18u}$$

$$\left(\widehat{K}_{ij}^{\eta},\bar{B}_{ij}^{\eta},\widehat{I}_{ij}^{\eta}\right)=\int_{-h/2}^{h/2}\left(\left(g''\left(z\right)\right)^{2},g''\left(z\right)g'\left(z\right),\left(g'\left(z\right)\right)^{2}\right)2\mu l_{2}^{2}dz \tag{18v}$$

where

$$\mathbf{Q}_{b}=\frac{E\left(z\right)}{1-\nu^{2}\left(z\right)}\begin{bmatrix}1 & \nu\left(z\right) & 0\\ \nu\left(z\right) & 1 & 0\\ 0 & 0 & \left(1-\nu\left(z\right)\right)/2\end{bmatrix};\ \mathbf{Q}_{s}=\frac{E\left(z\right)}{2\left(1+\nu\left(z\right)\right)}\begin{bmatrix}1 & 0\\ 0 & 1\end{bmatrix} \tag{19}$$

By using Hamilton's principle, the weak formulations of FG microplates based on MST are constructed systematically in accordance with general procedure of FEA [80] as follows

$$\int_{\Omega}\delta\hat{\boldsymbol{\varepsilon}}^{T}\hat{\mathbf{D}}_{\varepsilon}\hat{\boldsymbol{\varepsilon}}d\Omega+\int_{\Omega}\delta\hat{\boldsymbol{\varsigma}}^{T}\hat{\mathbf{D}}_{\varsigma}\hat{\boldsymbol{\varsigma}}d\Omega+\int_{\Omega}\delta\hat{\boldsymbol{\eta}}^{T}\hat{\mathbf{D}}_{\eta}\boldsymbol{\Gamma}_{\eta}\hat{\boldsymbol{\eta}}d\Omega+\int_{\Omega}\delta\hat{\boldsymbol{\chi}}^{T}\hat{\mathbf{D}}_{\chi}\boldsymbol{\Gamma}_{\chi}\hat{\boldsymbol{\chi}}d\Omega=\int_{\Omega}q\delta wd\Omega \tag{20a}$$

$$\int_{\Omega}\delta\hat{\boldsymbol{\varepsilon}}^{T}\hat{\mathbf{D}}_{\varepsilon}\hat{\boldsymbol{\varepsilon}}d\Omega+\int_{\Omega}\delta\hat{\boldsymbol{\varsigma}}^{T}\hat{\mathbf{D}}_{\varsigma}\hat{\boldsymbol{\varsigma}}d\Omega+\int_{\Omega}\delta\hat{\boldsymbol{\eta}}^{T}\hat{\mathbf{D}}_{\eta}\boldsymbol{\Gamma}_{\eta}\hat{\boldsymbol{\eta}}d\Omega+\int_{\Omega}\delta\hat{\boldsymbol{\chi}}^{T}\hat{\mathbf{D}}_{\chi}\boldsymbol{\Gamma}_{\chi}\hat{\boldsymbol{\chi}}d\Omega=\int_{\Omega}\delta\dot{\tilde{\mathbf{u}}}^{T}\mathbf{m}\dot{\tilde{\mathbf{u}}}d\Omega \tag{20b}$$

$$\int_{\Omega}\delta\hat{\boldsymbol{\varepsilon}}^{T}\hat{\mathbf{D}}_{\varepsilon}\hat{\boldsymbol{\varepsilon}}d\Omega+\int_{\Omega}\delta\hat{\boldsymbol{\varsigma}}^{T}\hat{\mathbf{D}}_{\varsigma}\hat{\boldsymbol{\varsigma}}d\Omega+\int_{\Omega}\delta\hat{\boldsymbol{\eta}}^{T}\hat{\mathbf{D}}_{\eta}\boldsymbol{\Gamma}_{\eta}\hat{\boldsymbol{\eta}}d\Omega+\int_{\Omega}\delta\hat{\boldsymbol{\chi}}^{T}\hat{\mathbf{D}}_{\chi}\boldsymbol{\Gamma}_{\chi}\hat{\boldsymbol{\chi}}d\Omega=\int_{\Omega}\nabla^{T}\delta w\mathbf{N}_{0}\nabla wd\Omega \tag{20c}$$

where Ω denotes the domain of the middle plane of the plate, $\tilde{\mathbf{u}}=\left\{\begin{array}{ccc}\tilde{\mathbf{u}}_{1} & \tilde{\mathbf{u}}_{2} & \tilde{\mathbf{u}}_{3}\end{array}\right\}^{T}$, $\mathbf{m}$ is the mass matrix, $\nabla^{T}=\left\{\begin{array}{cc}\frac{\partial}{\partial x} & \frac{\partial}{\partial y}\end{array}\right\}$, $\mathbf{N}_{0}$ is the matrix of pre-buckling load, $\boldsymbol{\Gamma}_{\eta}$ and $\boldsymbol{\Gamma}_{\chi}$ are diagonal matrices of coefficients. Details of $\tilde{\mathbf{u}}$, $\mathbf{m}$, $\mathbf{N}_{0}$, $\boldsymbol{\Gamma}_{\eta}$ and $\boldsymbol{\Gamma}_{\chi}$ are given below

$$\tilde{\mathbf{u}}_{1}=\left\{\begin{array}{c}u\\ v\\ w\end{array}\right\};\tilde{\mathbf{u}}_{2}=\left\{\begin{array}{c}\theta_{x}\\ \theta_{y}\\ 0\end{array}\right\};\tilde{\mathbf{u}}_{3}=\left\{\begin{array}{c}-\frac{\partial w}{\partial x}\\ -\frac{\partial w}{\partial y}\\ 0\end{array}\right\} \tag{21}$$

$$\mathbf{m}=\begin{bmatrix}I_{1} & I_{2} & I_{3}\\ I_{3} & I_{4} & I_{5}\\ I_{3} & I_{5} & I_{6}\end{bmatrix} \tag{22a}$$

where

$$\left(I_{1},I_{2},I_{3},I_{4},I_{5},I_{6}\right)=\int_{-h/2}^{h/2}\rho_{e}\left(z\right)\left(1,f\left(z\right),g\left(z\right),\left(f\left(z\right)\right)^{2},f\left(z\right)g\left(z\right),\left(g\left(z\right)\right)^{2}\right)dz \tag{22b}$$

$$\mathbf{N}_{0}=\begin{bmatrix}N_{x}^{0} & N_{xy}^{0}\\ N_{xy}^{0} & N_{y}^{0}\end{bmatrix} \tag{23}$$

$$diag\left(\boldsymbol{\Gamma}_{\eta}\right)=\left\{\begin{array}{ccccccccccc}1 & 1 & 1 & 3 & 3 & 3 & 6 & 1 & 1 & 1\end{array}\right\} \tag{24}$$

and

$$diag\left(\boldsymbol{\Gamma}_{\chi}\right)=\left\{\begin{array}{cccccc}1 & 1 & 2 & 1 & 2 & 2\end{array}\right\} \tag{25}$$

3. Isogeometric formulation

3.1. Brief review of NURBS-based IGA

A so-called knot vector Ξ is the fundamental component in the IGA and defined as a set of non-decreasing numbers:

$$\Xi = \{\xi_1,\ \xi_2,\ \xi_3, ...,\ \xi_i, ...,\ \xi_{n+p+1}\},\ \xi_i \leq \xi_{i+1} \tag{26}$$

where ξ_i denotes the i^{th} knot with i=1, 2, ...,n + p + 1; n being the number of basis functions, and p being the order of B-spline basis functions. The intervals [ξ_1, ξ_{n+p+1}] and [ξ_i, ξ_{i+1}) are called patch and knot span, respectively. An open and uniform knot vector is the one that the first and last knot have the multiplicity of p+1 and other knots are in uniform arrangement.

To construct the B-spline basis functions $N_{i,0}(\xi)$ with a given knot vector, the recursively procedure of Cox-de Boor formula is employed, where the process commences with p = 0

$$N_{i,0}(\xi) = \begin{cases} 1 & \xi_i \leq \xi < \xi_{i+1} \\ 0 & \text{otherwise} \end{cases} \tag{27}$$

then, for $p \geq 1$,

$$N_{i,p} = \frac{\xi - \xi_i}{\xi_{i+p} - \xi_i} N_{i,p-1}(\xi) + \frac{\xi_{i+p+1} - \xi}{\xi_{i+p+1} - \xi_{i+1}} N_{i,p-1}(\xi) \tag{28}$$

Here, an assumption of the fraction 0/0 = 0 is prescribed. Similar to the interpolation functions in the traditional FEA, the B-spline basis functions are linear independent and constitute the partition of unity. However, the B-splines basis functions are also non-negative in over parametric domain, $C^{\infty}-$continuous inside a knot span and $C^{p-k}-$continuous at the knots have multiplicity of k.

The NURBS basis functions for 2-D problems $R^{p}_{i,j}(\xi, \eta)$ are generated based on a tensor product of two univariate B-spline basis functions $N_{i,p}(\xi)$ and $M_{j,p}(\eta)$ as follows:

$$R^{p,q}_{i,j}(\xi, \eta) = \frac{N_{i,p}(\xi) M_{j,p}(\eta) w_{i,j}}{\sum_{\hat{i}=1}^{n} \sum_{\hat{j}=1}^{m} N_{\hat{i},p}(\xi) M_{\hat{j},p}(\eta) w_{\hat{i},\hat{j}}} \tag{29}$$

where $w_i > 0$ are the weight values introduced to exactly present the geometries of conical configurations.

For meshing purpose, there are three techniques were introduced in the IGA: *knot insertion* ($h-$ refinement), *order elevation* ($p-$ refinement) and advanced k-refinement. It is worth noticing that the k-refinement technique not only leaves the underlying geometry and its parameterization intact but also elevates the continuity of basis functions efficiently. Along with the ability to model exactly the geometries of any objects, these features make the IGA approach preferable in practice. For the numerical integrations, the well-known Gaussian quadrature is employed on knot spans and the number of Gauss points used to obtain the results is $(q+1)(p+1)$. More details of the NURBS basis functions and IGA procedures could be found in renowned books [81, 82].

3.2. NURBS-based formulation for MST plates

By employing the NURBS basis functions as the interpolation functions, the displacement variables are expressed by

$$\bar{\mathbf{u}} = \sum_{c}^{m\times n} R_c\left(\xi,\eta\right)\mathbf{d}_c \tag{30}$$

where $\bar{\mathbf{u}} = \left[\begin{array}{ccccc} u & v & \theta_x & \theta_y & w \end{array}\right]^T$. $\mathbf{d}_c = \left[\begin{array}{ccccc} u_c & v_c & \theta_{xc} & \theta_{yc} & w_c \end{array}\right]^T$ is the vector consisting degree of freedoms corresponding to the control point c, $m \times n$ denotes the numbers of control points associated with an element. By using Eq. (30), the strain tensor and other gradient tensors can be expressed as follows

$$\hat{\boldsymbol{\varepsilon}} = \left\{\begin{array}{c} \boldsymbol{\varepsilon}_0 \\ \boldsymbol{\varepsilon}_1 \\ \boldsymbol{\varepsilon}_2 \\ \boldsymbol{\gamma}_1 \\ \boldsymbol{\gamma}_2 \end{array}\right\} = \sum_{c}^{m\times n} \left\{\begin{array}{c} \mathbf{B}_{\varepsilon}^0 \\ \mathbf{B}_{\varepsilon}^1 \\ \mathbf{B}_{\varepsilon}^2 \\ \mathbf{B}_{\varepsilon}^3 \\ \mathbf{B}_{\varepsilon}^4 \end{array}\right\}_c \mathbf{d}_c;\ \hat{\boldsymbol{\varsigma}} = \left\{\begin{array}{c} \boldsymbol{\varsigma}_0 \\ \boldsymbol{\varsigma}_1 \\ \boldsymbol{\varsigma}_2 \\ \boldsymbol{\varsigma}_3 \\ \boldsymbol{\varsigma}_4 \end{array}\right\} = \sum_{c}^{m\times n} \left\{\begin{array}{c} \mathbf{B}_{\varsigma}^0 \\ \mathbf{B}_{\varsigma}^1 \\ \mathbf{B}_{\varsigma}^2 \\ \mathbf{B}_{\varsigma}^3 \\ \mathbf{B}_{\varsigma}^4 \end{array}\right\}_c \mathbf{d}_c \tag{31a}$$

$$\hat{\boldsymbol{\eta}} = \left\{\begin{array}{c} \boldsymbol{\eta}_0 \\ \boldsymbol{\eta}_1 \\ \boldsymbol{\eta}_2 \\ \boldsymbol{\eta}_3 \\ \boldsymbol{\eta}_4 \\ \boldsymbol{\eta}_5 \\ \boldsymbol{\eta}_6 \end{array}\right\} = \sum_{c}^{m\times n} \left\{\begin{array}{c} \mathbf{B}_{\eta}^0 \\ \mathbf{B}_{\eta}^1 \\ \mathbf{B}_{\eta}^2 \\ \mathbf{B}_{\eta}^3 \\ \mathbf{B}_{\eta}^4 \\ \mathbf{B}_{\eta}^5 \\ \mathbf{B}_{\eta}^6 \end{array}\right\}_c \mathbf{d}_c;\ \hat{\boldsymbol{\chi}} = \left\{\begin{array}{c} \boldsymbol{\chi}_0 \\ \boldsymbol{\chi}_1 \\ \boldsymbol{\chi}_2 \\ \boldsymbol{\chi}_3 \\ \boldsymbol{\chi}_4 \\ \boldsymbol{\chi}_5 \end{array}\right\} = \sum_{c}^{m\times n} \left\{\begin{array}{c} \mathbf{B}_{\chi}^0 \\ \mathbf{B}_{\chi}^1 \\ \mathbf{B}_{\chi}^2 \\ \mathbf{B}_{\chi}^3 \\ \mathbf{B}_{\chi}^4 \\ \mathbf{B}_{\chi}^5 \end{array}\right\}_c \mathbf{d}_c \tag{31b}$$

where

$$\mathbf{B}_{\varepsilon c}^0 = \left[\begin{array}{ccccc} \frac{\partial R_c}{\partial x} & 0 & 0 & 0 & 0 \\ 0 & \frac{\partial R_c}{\partial y} & 0 & 0 & 0 \\ \frac{\partial R_c}{\partial y} & \frac{\partial R_c}{\partial x} & 0 & 0 & 0 \end{array}\right]; \mathbf{B}_{\varepsilon c}^1 = \left[\begin{array}{ccccc} 0 & 0 & \frac{\partial R_c}{\partial x} & 0 & 0 \\ 0 & 0 & 0 & \frac{\partial R_c}{\partial y} & 0 \\ 0 & 0 & \frac{\partial R_c}{\partial y} & \frac{\partial R_c}{\partial x} & 0 \end{array}\right]; \mathbf{B}_{\varepsilon c}^2 = \left[\begin{array}{ccccc} 0 & 0 & 0 & 0 & -\frac{\partial^2 R_c}{\partial x^2} \\ 0 & 0 & 0 & 0 & -\frac{\partial^2 R_c}{\partial y^2} \\ 0 & 0 & 0 & 0 & -2\frac{\partial^2 R_c}{\partial x \partial y} \end{array}\right] \tag{32a}$$

$$\mathbf{B}_{\varepsilon c}^3 = \left[\begin{array}{ccccc} 0 & 0 & R_c & 0 & 0 \\ 0 & 0 & 0 & R_c & 0 \end{array}\right]; \mathbf{B}_{\varepsilon c}^4 = \left[\begin{array}{ccccc} 0 & 0 & 0 & 0 & \frac{\partial R_c}{\partial x} \\ 0 & 0 & 0 & 0 & \frac{\partial R_c}{\partial y} \end{array}\right] \tag{32b}$$

$$\mathbf{B}_{\varsigma c}^0 = \left[\begin{array}{ccccc} \frac{\partial^2 R_c}{\partial x^2} & \frac{\partial^2 R_c}{\partial x \partial y} & 0 & 0 & 0 \\ \frac{\partial^2 R_c}{\partial x \partial y} & \frac{\partial^2 R_c}{\partial y^2} & 0 & 0 & 0 \end{array}\right]; \mathbf{B}_{\varsigma c}^1 = \left[\begin{array}{ccccc} 0 & \frac{\partial^2 R_c}{\partial x^2} & \frac{\partial^2 R_c}{\partial x \partial y} & 0 & 0 \\ 0 & \frac{\partial^2 R_c}{\partial x \partial y} & \frac{\partial^2 R_c}{\partial y^2} & 0 & 0 \end{array}\right]; \mathbf{B}_{\varsigma c}^2 = \left[\begin{array}{ccccc} 0 & 0 & 0 & 0 & -\frac{\partial^3 R_c}{\partial x^3} - \frac{\partial^3 R_c}{\partial x \partial y^2} \\ 0 & 0 & 0 & 0 & -\frac{\partial^3 R_c}{\partial x^2 \partial y} - \frac{\partial^3 R_c}{\partial y^3} \end{array}\right] \tag{32c}$$

$$\mathbf{B}_{\varsigma c}^3 = \left[\begin{array}{ccccc} 0 & 0 & \frac{\partial R_c}{\partial x} & \frac{\partial R_c}{\partial y} & 0 \end{array}\right]; \mathbf{B}_{\varsigma c}^4 = \left[\begin{array}{ccccc} 0 & 0 & 0 & 0 & -\frac{\partial^2 R_c}{\partial x^2} - \frac{\partial^2 R_c}{\partial y^2} \end{array}\right] \tag{32d}$$

$$\mathbf{B}^0_{\eta c} = \begin{bmatrix} \frac{2}{5}\frac{\partial^2 R_c}{\partial x^2} - \frac{1}{5}\frac{\partial^2 R_c}{\partial y^2} & -\frac{2}{5}\frac{\partial^2 R_c}{\partial x \partial y} & 0 & 0 & 0 \\ -\frac{2}{5}\frac{\partial^2 R_c}{\partial x \partial y} & \frac{2}{5}\frac{\partial^2 R_c}{\partial y^2} - \frac{1}{5}\frac{\partial^2 R_c}{\partial x^2} & 0 & 0 & 0 \\ 0 & 0 & 0 & 0 & -\frac{1}{5}\frac{\partial^2 R_c}{\partial x^2} - \frac{1}{5}\frac{\partial^2 R_c}{\partial y^2} \\ \frac{8}{15}\frac{\partial^2 R_c}{\partial x \partial y} & \frac{4}{15}\frac{\partial^2 R_c}{\partial x^2} - \frac{1}{5}\frac{\partial^2 R_c}{\partial y^2} & 0 & 0 & 0 \\ 0 & 0 & 0 & 0 & \frac{4}{15}\frac{\partial^2 R_c}{\partial x^2} - \frac{1}{15}\frac{\partial^2 R_c}{\partial y^2} \\ \frac{4}{15}\frac{\partial^2 R_c}{\partial y^2} - \frac{1}{5}\frac{\partial^2 R_c}{\partial x^2} & \frac{8}{15}\frac{\partial^2 R_c}{\partial x \partial y} & 0 & 0 & 0 \\ 0 & 0 & 0 & 0 & \frac{1}{3}\frac{\partial^2 R_c}{\partial x \partial y} \\ -\frac{1}{5}\frac{\partial^2 R_c}{\partial x^2} - \frac{1}{15}\frac{\partial^2 R_c}{\partial y^2} & -\frac{2}{15}\frac{\partial^2 R_c}{\partial x \partial y} & 0 & 0 & 0 \\ 0 & 0 & 0 & 0 & -\frac{1}{15}\frac{\partial^2 R_c}{\partial x^2} + \frac{4}{15}\frac{\partial^2 R_c}{\partial y^2} \\ -\frac{2}{15}\frac{\partial^2 R_c}{\partial x \partial y} & -\frac{1}{15}\frac{\partial^2 R_c}{\partial x^2} - \frac{1}{5}\frac{\partial^2 R_c}{\partial y^2} & 0 & 0 & 0 \end{bmatrix} \tag{32e}$$

$$\mathbf{B}^1_{\eta c} = \begin{bmatrix} 0 & 0 & -\frac{1}{5}R_c & 0 & 0 \\ 0 & 0 & 0 & -\frac{1}{5}R_c & 0 \\ 0 & 0 & 0 & 0 & 0 \\ 0 & 0 & 0 & -\frac{1}{15}R_c & 0 \\ 0 & 0 & 0 & 0 & 0 \\ 0 & 0 & -\frac{1}{15}R_c & 0 & 0 \\ 0 & 0 & 0 & 0 & 0 \\ 0 & 0 & \frac{4}{15}R_c & 0 & 0 \\ 0 & 0 & 0 & 0 & 0 \\ 0 & 0 & 0 & \frac{4}{15}R_c & 0 \end{bmatrix}; \mathbf{B}^2_{\eta c} = \begin{bmatrix} 0 & 0 & 0 & 0 & 0 \\ 0 & 0 & 0 & 0 & 0 \\ 0 & 0 & -\frac{2}{5}\frac{\partial R_c}{\partial x} & -\frac{2}{5}\frac{\partial R_c}{\partial y} & 0 \\ 0 & 0 & 0 & 0 & 0 \\ 0 & 0 & \frac{8}{15}\frac{\partial R_c}{\partial x} & -\frac{2}{15}\frac{\partial R_c}{\partial y} & 0 \\ 0 & 0 & 0 & 0 & 0 \\ 0 & 0 & \frac{1}{3}\frac{\partial R_c}{\partial y} & \frac{1}{3}\frac{\partial R_c}{\partial x} & 0 \\ 0 & 0 & 0 & 0 & 0 \\ 0 & 0 & -\frac{2}{15}\frac{\partial R_c}{\partial x} & \frac{8}{15}\frac{\partial R_c}{\partial y} & 0 \\ 0 & 0 & 0 & 0 & 0 \end{bmatrix} \tag{32f}$$

$$\mathbf{B}^3_{\eta c} = \begin{bmatrix} 0 & 0 & \frac{2}{5}\frac{\partial^2 R_c}{\partial x^2} - \frac{1}{5}\frac{\partial^2 R_c}{\partial y^2} & -\frac{2}{5}\frac{\partial^2 R_c}{\partial x \partial y} & 0 \\ 0 & 0 & -\frac{2}{5}\frac{\partial^2 R_c}{\partial x \partial y} & \frac{2}{5}\frac{\partial^2 R_c}{\partial y^2} - \frac{1}{5}\frac{\partial^2 R_c}{\partial x^2} & 0 \\ 0 & 0 & 0 & 0 & 0 \\ 0 & 0 & \frac{8}{15}\frac{\partial^2 R_c}{\partial x \partial y} & \frac{4}{15}\frac{\partial^2 R_c}{\partial x^2} - \frac{1}{5}\frac{\partial^2 R_c}{\partial y^2} & 0 \\ 0 & 0 & 0 & 0 & 0 \\ 0 & 0 & -\frac{1}{5}\frac{\partial^2 R_c}{\partial x^2} & \frac{4}{15}\frac{\partial^2 R_c}{\partial y^2} + \frac{8}{15}\frac{\partial^2 R_c}{\partial x \partial y} & 0 \\ 0 & 0 & 0 & 0 & 0 \\ 0 & 0 & -\frac{1}{5}\frac{\partial^2 R_c}{\partial x^2} - \frac{1}{15}\frac{\partial^2 R_c}{\partial y^2} & -\frac{2}{15}\frac{\partial^2 R_c}{\partial x \partial y} & 0 \\ 0 & 0 & 0 & 0 & 0 \\ 0 & 0 & -\frac{2}{15}\frac{\partial^2 R_c}{\partial x \partial y} & -\frac{1}{15}\frac{\partial^2 R_c}{\partial x^2} - \frac{1}{5}\frac{\partial^2 R_c}{\partial y^2} & 0 \end{bmatrix}; \mathbf{B}^4_{\eta c} = \begin{bmatrix} 0 & 0 & 0 & 0 & \frac{1}{5}\frac{\partial R_c}{\partial x} \\ 0 & 0 & 0 & 0 & \frac{1}{5}\frac{\partial R_c}{\partial y} \\ 0 & 0 & 0 & 0 & 0 \\ 0 & 0 & 0 & 0 & \frac{1}{15}\frac{\partial R_c}{\partial y} \\ 0 & 0 & 0 & 0 & 0 \\ 0 & 0 & 0 & 0 & \frac{1}{15}\frac{\partial R_c}{\partial x} \\ 0 & 0 & 0 & 0 & 0 \\ 0 & 0 & 0 & 0 & -\frac{4}{15}\frac{\partial R_c}{\partial x} \\ 0 & 0 & 0 & 0 & 0 \\ 0 & 0 & 0 & 0 & -\frac{4}{15}\frac{\partial R_c}{\partial y} \end{bmatrix} \tag{32g}$$

$$\mathbf{B}_{\eta c}^{5}=\begin{bmatrix} 0 & 0 & 0 & 0 & 0 \\ 0 & 0 & 0 & 0 & 0 \\ 0 & 0 & 0 & 0 & \frac{2}{5}\frac{\partial^2 R_c}{\partial x^2}+\frac{2}{5}\frac{\partial^2 R_c}{\partial y^2} \\ 0 & 0 & 0 & 0 & 0 \\ 0 & 0 & 0 & 0 & -\frac{8}{15}\frac{\partial^2 R_c}{\partial x^2}+\frac{2}{15}\frac{\partial^2 R_c}{\partial y^2} \\ 0 & 0 & 0 & 0 & 0 \\ 0 & 0 & 0 & 0 & -\frac{1}{2}\frac{\partial^2 R_c}{\partial x \partial y} \\ 0 & 0 & 0 & 0 & 0 \\ 0 & 0 & 0 & 0 & \frac{2}{15}\frac{\partial^2 R_c}{\partial x^2}-\frac{8}{15}\frac{\partial^2 R_c}{\partial y^2} \\ 0 & 0 & 0 & 0 & 0 \end{bmatrix};\mathbf{B}_{\eta c}^{6}=\begin{bmatrix} 0 & 0 & 0 & 0 & -\frac{2}{5}\frac{\partial^3 R_c}{\partial x^3}+\frac{3}{5}\frac{\partial^3 R_c}{\partial x \partial y^2} \\ 0 & 0 & 0 & 0 & -\frac{2}{5}\frac{\partial^3 R_c}{\partial y^3}+\frac{3}{5}\frac{\partial^3 R_c}{\partial x^2 \partial y} \\ 0 & 0 & 0 & 0 & 0 \\ 0 & 0 & 0 & 0 & -\frac{4}{5}\frac{\partial^3 R_c}{\partial x^2 \partial y}+\frac{1}{5}\frac{\partial^3 R_c}{\partial y^3} \\ 0 & 0 & 0 & 0 & 0 \\ 0 & 0 & 0 & 0 & \frac{1}{5}\frac{\partial^3 R_c}{\partial x^3}-\frac{4}{5}\frac{\partial^3 R_c}{\partial x \partial y^2} \\ 0 & 0 & 0 & 0 & 0 \\ 0 & 0 & 0 & 0 & \frac{1}{5}\frac{\partial^3 R_c}{\partial x^3}+\frac{1}{5}\frac{\partial^3 R_c}{\partial x \partial y^2} \\ 0 & 0 & 0 & 0 & 0 \\ 0 & 0 & 0 & 0 & \frac{1}{5}\frac{\partial^3 R_c}{\partial x^2 \partial y}+\frac{1}{5}\frac{\partial^3 R_c}{\partial y^3} \end{bmatrix} \tag{32h}$$

$$\mathbf{B}_{\chi c}^{0}=\begin{bmatrix} 0 & 0 & 0 & 0 & \frac{1}{2}\frac{\partial^2 R_c}{\partial x \partial y} \\ 0 & 0 & 0 & 0 & -\frac{1}{2}\frac{\partial^2 R_c}{\partial x \partial y} \\ 0 & 0 & 0 & 0 & \frac{1}{4}\frac{\partial^2 R_c}{\partial y^2}-\frac{1}{4}\frac{\partial^2 R_c}{\partial x^2} \\ 0 & 0 & 0 & 0 & 0 \\ -\frac{1}{4}\frac{\partial^2 R_c}{\partial x \partial y} & \frac{1}{4}\frac{\partial^2 R_c}{\partial x^2} & 0 & 0 & 0 \\ -\frac{1}{4}\frac{\partial^2 R_c}{\partial y^2} & \frac{1}{4}\frac{\partial^2 R_c}{\partial x \partial y} & 0 & 0 & 0 \end{bmatrix};\mathbf{B}_{\chi c}^{1}=\begin{bmatrix} 0 & 0 & 0 & 0 & 0 \\ 0 & 0 & 0 & 0 & 0 \\ 0 & 0 & 0 & 0 & 0 \\ 0 & 0 & 0 & 0 & 0 \\ 0 & 0 & 0 & -\frac{1}{4}R_c & 0 \\ 0 & 0 & \frac{1}{4}R_c & 0 & 0 \end{bmatrix} \tag{32i}$$

$$\mathbf{B}_{\chi c}^{2}=\begin{bmatrix} 0 & 0 & 0 & -\frac{1}{2}\frac{\partial R_c}{\partial x} & 0 \\ 0 & 0 & \frac{1}{2}\frac{\partial R_c}{\partial y} & 0 & 0 \\ 0 & 0 & \frac{1}{4}\frac{\partial R_c}{\partial x} & -\frac{1}{4}\frac{\partial R_c}{\partial y} & 0 \\ 0 & 0 & -\frac{1}{2}\frac{\partial R_c}{\partial y} & \frac{1}{2}\frac{\partial R_c}{\partial x} & 0 \\ 0 & 0 & 0 & 0 & 0 \\ 0 & 0 & 0 & 0 & 0 \end{bmatrix};\mathbf{B}_{\chi c}^{3}=\begin{bmatrix} 0 & 0 & 0 & 0 & 0 \\ 0 & 0 & 0 & 0 & 0 \\ 0 & 0 & 0 & 0 & 0 \\ 0 & 0 & 0 & 0 & 0 \\ 0 & 0 & -\frac{1}{4}\frac{\partial^2 R_c}{\partial x \partial y} & \frac{1}{4}\frac{\partial^2 R_c}{\partial x^2} & 0 \\ 0 & 0 & -\frac{1}{4}\frac{\partial^2 R_c}{\partial y^2} & \frac{1}{4}\frac{\partial^2 R_c}{\partial x \partial y} & 0 \end{bmatrix} \tag{32j}$$

$$\mathbf{B}_{\chi c}^{4}=\begin{bmatrix} 0 & 0 & 0 & 0 & 0 \\ 0 & 0 & 0 & 0 & 0 \\ 0 & 0 & 0 & 0 & 0 \\ 0 & 0 & 0 & 0 & 0 \\ 0 & 0 & 0 & 0 & \frac{1}{4}\frac{\partial R_c}{\partial y} \\ 0 & 0 & 0 & 0 & -\frac{1}{4}\frac{\partial R_c}{\partial x} \end{bmatrix};\mathbf{B}_{\chi c}^{5}=\begin{bmatrix} 0 & 0 & 0 & 0 & \frac{1}{2}\frac{\partial^2 R_c}{\partial x \partial y} \\ 0 & 0 & 0 & 0 & -\frac{1}{2}\frac{\partial^2 R_c}{\partial x \partial y} \\ 0 & 0 & 0 & 0 & \frac{1}{4}\frac{\partial^2 R_c}{\partial y^2}-\frac{1}{4}\frac{\partial^2 R_c}{\partial x^2} \\ 0 & 0 & 0 & 0 & 0 \\ 0 & 0 & 0 & 0 & 0 \\ 0 & 0 & 0 & 0 & 0 \end{bmatrix} \tag{32k}$$

Next, substituting Eq. (31) into Eq. (20), the NURBS-based formulations for static bending, vibration and buckling analyses of FG microplates based on the MST are obtained. For the static bending problems, the global system equation is expressed by

$$\left(\mathbf{K}_{\varepsilon}+\mathbf{K}_{\varsigma}+\mathbf{K}_{\eta}+\mathbf{K}_{\chi}\right)\mathbf{d}=\mathbf{f} \tag{33}$$

where $\mathbf{K}_\varepsilon, \mathbf{K}_\varsigma, \mathbf{K}_\eta$ and $\mathbf{K}_\chi$ are the stiffness matrices regarding to the strain tensor ε_{ij}, dilatation gradient tensor ς_i, deviatoric stretch gradient tensor $\eta^{(1)}_{ijk}$ and symmetric part of rotation gradient tensor χ^s_{ij}, respectively. $\mathbf{f}$ denotes the vector of external distributed load. Details of those are given by

$$\mathbf{K}_\varepsilon = \int_\Omega \mathbf{B}^T_{\varepsilon T} \hat{\mathbf{D}}_\varepsilon \mathbf{B}_{\varepsilon T} d\Omega;\ \mathbf{K}_\varsigma = \int_\Omega \mathbf{B}^T_{\varsigma T} \hat{\mathbf{D}}_\varsigma \mathbf{B}_\varsigma d\Omega \tag{34a}$$

$$\mathbf{K}_\eta = \int_\Omega \mathbf{B}^T_{\eta T} \hat{\mathbf{D}}_\eta \mathbf{\Gamma}_\eta \mathbf{B}_\eta d\Omega;\ \mathbf{K}_\chi = \int_\Omega \mathbf{B}^T_{\chi T} \hat{\mathbf{D}}_\chi \mathbf{\Gamma}_\chi \mathbf{B}_\chi d\Omega \tag{34b}$$

in which

$$\mathbf{B}_\varepsilon = \begin{Bmatrix} \mathbf{B}^0_\varepsilon \\ \mathbf{B}^1_\varepsilon \\ \mathbf{B}^2_\varepsilon \\ \mathbf{B}^3_\varepsilon \\ \mathbf{B}^4_\varepsilon \end{Bmatrix}; \mathbf{B}_{\varepsilon T} = \begin{Bmatrix} (\mathbf{B}^0_\varepsilon)^T \\ (\mathbf{B}^1_\varepsilon)^T \\ (\mathbf{B}^2_\varepsilon)^T \\ (\mathbf{B}^3_\varepsilon)^T \\ (\mathbf{B}^4_\varepsilon)^T \end{Bmatrix}; \mathbf{B}_\varsigma = \begin{Bmatrix} \mathbf{B}^0_\varsigma \\ \mathbf{B}^1_\varsigma \\ \mathbf{B}^2_\varsigma \\ \mathbf{B}^3_\varsigma \\ \mathbf{B}^4_\varsigma \end{Bmatrix}; \mathbf{B}_{\varsigma T} = \begin{Bmatrix} \left(\mathbf{B}^0_\varsigma\right)^T \\ \left(\mathbf{B}^1_\varsigma\right)^T \\ \left(\mathbf{B}^2_\varsigma\right)^T \\ \left(\mathbf{B}^3_\varsigma\right)^T \\ \left(\mathbf{B}^4_\varsigma\right)^T \end{Bmatrix} \tag{34c}$$

$$\mathbf{B}_\eta = \begin{Bmatrix} \mathbf{B}^0_\eta \\ \mathbf{B}^1_\eta \\ \mathbf{B}^2_\eta \\ \mathbf{B}^3_\eta \\ \mathbf{B}^4_\eta \\ \mathbf{B}^5_\eta \\ \mathbf{B}^6_\eta \end{Bmatrix}; \mathbf{B}_{\eta T} = \begin{Bmatrix} \left(\mathbf{B}^0_\eta\right)^T \\ \left(\mathbf{B}^1_\eta\right)^T \\ \left(\mathbf{B}^2_\eta\right)^T \\ \left(\mathbf{B}^3_\eta\right)^T \\ \left(\mathbf{B}^4_\eta\right)^T \\ \left(\mathbf{B}^5_\eta\right)^T \\ \left(\mathbf{B}^6_\eta\right)^T \end{Bmatrix}; \mathbf{B}_\chi = \begin{Bmatrix} \mathbf{B}^0_\chi \\ \mathbf{B}^1_\chi \\ \mathbf{B}^2_\chi \\ \mathbf{B}^3_\chi \\ \mathbf{B}^4_\chi \\ \mathbf{B}^5_\chi \end{Bmatrix} \mathbf{B}_{\chi T} = \begin{Bmatrix} \left(\mathbf{B}^0_\chi\right)^T \\ \left(\mathbf{B}^1_\chi\right)^T \\ \left(\mathbf{B}^2_\chi\right)^T \\ \left(\mathbf{B}^3_\chi\right)^T \\ \left(\mathbf{B}^4_\chi\right)^T \\ \left(\mathbf{B}^5_\chi\right)^T \end{Bmatrix} \tag{34d}$$

and

$$\mathbf{f} = \int_\Omega q\left(x, y\right) \begin{bmatrix} 0 & 0 & 0 & 0 & R_c \end{bmatrix}^T d\Omega \tag{34e}$$

For the free vibration and buckling analyses, the system equations are given by

$$\left(\mathbf{K}_\varepsilon + \mathbf{K}_\varsigma + \mathbf{K}_\eta + \mathbf{K}_\chi - \omega^2 \mathbf{M}\right) \mathbf{d} = \mathbf{0} \tag{35a}$$

$$\left(\mathbf{K}_\varepsilon + \mathbf{K}_\varsigma + \mathbf{K}_\eta + \mathbf{K}_\chi - \lambda_{cr} \mathbf{K}_g\right) \mathbf{d} = \mathbf{0} \tag{35b}$$

where ω and λ_{cr} are the values of natural frequency and critical buckling load, respectively. $\mathbf{M}$ and $\mathbf{K}_g$ are the global mass matrix and geometric stiffness matrix.

$$\mathbf{M} = \int_\Omega \mathbf{R}^T_m \mathbf{m} \mathbf{R}_m d\Omega \tag{36}$$

in which

$$\mathbf{R_m} = \left\{ \begin{array}{c} \mathbf{R}_m^1 \\ \mathbf{R}_m^2 \\ \mathbf{R}_m^3 \end{array} \right\}; \mathbf{R}_{mc}^1 = \left[\begin{array}{ccccc} R_c & 0 & 0 & 0 & 0 \\ 0 & R_c & 0 & 0 & 0 \\ 0 & 0 & 0 & 0 & R_c \end{array} \right] \tag{37a}$$

$$\mathbf{R}_{mc}^2 = \left[\begin{array}{ccccc} 0 & 0 & R_c & 0 & 0 \\ 0 & 0 & 0 & R_c & 0 \\ 0 & 0 & 0 & 0 & 0 \end{array} \right]; \mathbf{R}_{mc}^3 = \left[\begin{array}{ccccc} 0 & 0 & 0 & 0 & -\frac{\partial R_c}{\partial x} \\ 0 & 0 & 0 & 0 & -\frac{\partial R_c}{\partial y} \\ 0 & 0 & 0 & 0 & 0 \end{array} \right] \tag{37b}$$

$$\mathbf{K}_g = \int_\Omega \mathbf{B}_g^T \mathbf{N}_0 \mathbf{B}_g d\Omega \tag{38}$$

where

$$\mathbf{B}_{gc} = \left[\begin{array}{ccccc} 0 & 0 & 0 & 0 & \frac{\partial R_c}{\partial x} \\ 0 & 0 & 0 & 0 & \frac{\partial R_c}{\partial y} \end{array} \right] \tag{39}$$

It is worth noticing from the NURBS-based formulations that the third-order derivatives of basis functions are needed to be performed in the constructions of the stiffness matrices. Consequently, C^2-continuous approximations are in demand. In the traditional FEA, this requirement would cause troublesome matters regarding the mesh-generations or constructions of the interpolation functions, which result in a tremendous cost of computational effort [42]. With the introduction of advanced $k-$refinement technique in the IGA, the continuity of basis functions are elevated efficiently as mentioned earlier. For the C^2-continuous requirement, the NURBS basis functions with order of $p \geq 3$ are adopted in this study.

4. Numerical examples

In this sections, numerical studies on static bending, free vibration and buckling of FG microplates are presented to validate the reliability of present MST plate model. Both rectangular and circular FG microplates are taken into investigation. Unless stated otherwise, the FG microplates are assumed to be made of Al/SiC materials where the bottom surface is metal-rich (Al) and the top surface is ceramic-rich (SiC). The material properties for Al are E_m = 70 GPa, ν_m = 0.3, ρ_m = 2702 kg/m^3, and for SiC are E_c = 380 GPa, ν_c = 0.3, ρ_c = 3800 kg/m^3. For simplification purpose, all three length scale parameters are assumed to have identical values $l_0 = l_1 = l_2 = l$. In general, the material length scale parameters should be determined through experimental data. Nevertheless, there is no available information regarding to the length scale parameter of FGM so far. Therefore, a conservative assumption of l = 15 μm is used in this study for FG microplates. For the shake of convenience, the following normalized quantities are used unless otherwise stated:

For the rectangular microplates

$$\bar{w} = \frac{10E_c h^3}{q_0 a^4} w\left(\frac{a}{2}, \frac{b}{2}\right); \bar{\omega} = \omega \frac{a^2}{h}\sqrt{\frac{\rho_c}{E_c}};\ \bar{\lambda}_{cr} = \lambda_{cr}\frac{a^2}{E_m h^3} \tag{40}$$

For the circular microplates

$$\bar{w} = \frac{64D_c}{q_0 r^4} w\left(0,0\right);\ \bar{\omega} = \omega r^2\sqrt{\frac{\rho_c h}{D_c}};\ \bar{\lambda}_{cr} = \lambda_{cr}\frac{r^2}{D_c} \tag{41}$$

where $D_c = E_c h^3/[12\left(1-\nu_c^2\right)]$ and r is the radius of the circular plate.

Several types of boundary conditions are considered, such as simply supported (SSSS), clamped (CCCC), simply supported and clamped (SCSC), and simply supported and free (SFSF) for the rectangular FG microplates as well as simply supported (Sr), roller (Rr), and clamped (Cr) for the circular FG microplates, respectively. The first two letters of each boundary conditions for the rectangular plates refer to that in the width ($y-$direction) and the length ($x-$direction). Details of those boundary conditions are given below:

SSSS

$$u = \theta_x = w = 0 \text{ at } y = 0 \text{ and } y = b \tag{42a}$$

$$v = \theta_y = w = 0 \text{ at } x = 0 \text{ and } x = a \tag{42b}$$

CCCC

$$u = v = \theta_x = \theta_y = w = \frac{\partial w}{\partial n} = 0 \text{ at all edges} \tag{43}$$

SCSC

$$u = \theta_x = w = 0 \text{ at } y = 0 \text{ and } y = b \tag{44a}$$

$$u = v = \theta_x = \theta_y = w = 0 \text{ at } x = 0 \text{ and } x = a \tag{44b}$$

SFSF

$$u = \theta_x = w = 0 \text{ at } y = 0 \text{ and } y = b \tag{45}$$

Sr

$$u = v = w = 0 \text{ at the boundary} \tag{46}$$

Rr

$$w = 0 \text{ at the boundary} \tag{47}$$

Cr

$$u = v = \theta_x = \theta_y = w = \frac{\partial w}{\partial n} = 0 \text{ at the boundary} \tag{48}$$

where $\frac{\partial}{\partial n}$ denotes the normal derivative operator. It is treated in the IGA by imposing zero values for transverse displacement in all control points in the boundary and those adjacent to them [83].

4.1. Convergence and verification studies

Table 1 presents the results for center displacements of homogeneous rectangular microplates under uniformly distributed load with different degrees of refinements. The microplates are assumed to be made of epoxy with the material properties as follows: E = 1.44 GPa, ν = 0.38, $a = b = 50h$, $l = h$ = 17.6 μm. The intensity of the uniformly distributed load is q = 1 kN/m^2. The results are compared with those obtained using the finite strip method [50] and approximately analytical solutions [42]. Various size meshes, which are from smaller to bigger than length scale parameter, are chosen. It can be seen that the present solutions quickly converge with $p \geq 3$ and the results are completely stable when the fourth-order basis functions $(p = 4)$ are employed along with (8×8) mesh. Therefore, this mesh is adopted in the remaining calculations. It should be noted that in this case the mesh size is bigger than length scale parameter. It implies that mesh size is not a concern for present approach, which is consistent with the observations from previous studies [76, 77] using non-local elasticity theory and the MCT. Illustrations for the meshes of rectangular and circular plates are depicted in Fig. 2. As can be seen in Table 1, the current results are in good agreement with the referenced ones. A slight discrepancy could be attributed to the distinction between the third-order shear deformation plate theory employed in this study and the Kirchhoff plate theory used in those referenced work, where the shear deformation effect is neglected.

The versatility of present model can be proved by setting $l_0 = l_1 = 0;\ l_2 = l$, which means that the results for the MCT are easily obtained. The displacements, natural frequencies and critical buckling loads of simply supported square FG microplates are compared with those from the literature using the MCT in Tables 2-4. The microplates investigated in bending and vibration responses are made of Al/SiC, whereas the material properties used in buckling problem are E_c = 14.4 GPa, E_m = 1.44 GPa and $\nu_c = \nu_m$ = 0.38. It can be seen that the present results are virtually identical with analytical solutions in Refs. [84] and [85]. In order to study the size effect in the MCT and MST, the results for bending, vibration and buckling problems for both theories are plotted in Fig. 3. The values in the vertical axis are the ratios of the results obtained from the MST to those from the MCT. It is obvious to see that the MST with three length scale parameters produces smaller displacements and higher frequencies and buckling loads than the MCT with only one length scale parameter. In other words, the size-dependent of MST is stronger than MCT for microplates especially when their thickness is close to the length scale parameter. It emphasises the important of the consideration of three components e.g. the dilatation, deviatoric stretch and symmetric part of rotation gradient tensor in the MST rather than only the symmetric part of rotation gradient tensor in the MCT when dealing with microplates. As expected, by increasing the size scale, the ratios of the results obtained from

MST to those from MCT become unity.

In order to further verify the reliability and versatility of the present MST model, simply supported square FG microplates and three types of circular FG microplates, which are simply supported (Sr), roller (Rr) and clamped (Cr), are considered. The results for displacements, natural frequencies and critical buckling loads of these microplates are presented and compared with those obtained by Zhang et al. [46, 47] in Tables 5- 10. $h/l = \infty$ denotes the classical theory which the size effect is totally neglected. It is observed that a good agreement between the present results and those from references is archived. As expected, the displacements predicted by the MST are always smaller than those of classical theory, whereas the natural frequencies and buckling loads of the former theory are larger than those of the latter one. It should be noted that Zhang et al. [46, 47] used two types of coordinates systems such as the Cartesian coordinate for square microplates and the polar coordinate for circular microplates to solve the problems. It clearly shows the prominent feature of IGA in this study since only Cartesian coordinate is used when dealing with both circular and rectangular microplates. Fig. 4 displays the variation of displacements, natural frequencies and buckling loads of circular microplates with different values of h/l for various boundary conditions. For the Rr and Sr circular microplates, it is interesting to see that the discrepancy of their displacements is negligible when the size effect is most significant and becomes bigger as h/l increases. However, their natural frequencies and buckling loads are nearly identical for any degrees of size effect (Figs. 4b, 4c). For the same boundary conditions, the size effect is more pronounced for buckling analysis than bending and vibration one. It also plays more important role for the clamped boundary conditions than the other two. The bending deformation and mode shapes for vibration and buckling analysis of circular FG micoplates with different boundary conditions are illustrated in Figs. 5-7.

4.2. Parametric study

In this section, the square FG microplates with various boundary conditions such as CCCC, SCSC and SFSF are considered. Since there is no study for bending, vibration and buckling analysis of these FG microplates using the MST reported in the literature, all the results are presented herein as benchmark tests for future references.

4.2.1. Static bending analysis

The normalized displacements of FG microplates under sinusoidally distributed load are given in Table 11. Figs. 8 and 9a also illustrate their variation with respect to the size effect, gradient index and thickness ratio. The results increase not only when the gradient index and size effect increase but also when thickness ratio decreases. Besides, they also increase as fewer clamped edges are considered. It

is clear that the FG microplate with the gradient index n = 0 (ceramic), thickness ratio a/h = 100 and all-clamped boundary conditions yield the smallest results (Figs. 8 and 9a). This is due to the fact that the two latter changes result in an increase in the metal phrase in the plate volume, shear deformation effect, respectively, whereas the last effect provides more free degree of freedoms. Furthermore, the displacements rise with the increment of h/l and become close to those obtained from classical cases when h/l is relative large (h/l = 20) as depicted in Figs. 8 and 9a. When $h/l < 10$, they decrease remarkably and their minimum results are obtained when h/l = 1. In other words, when the plates are on micron size and their thickness is close to the length scale parameter, the size effect becomes most considerable and tends to significantly reinforce the stiffness of the microplates, which consequently produces smaller displacements compared to the classical theory where size effect is not accounted. Additionally, it worth noting that the size effect tends to reduce the discrepancies between the results obtained from different cases of gradient index n, thickness ratios and boundary conditions. For example, the differences between the results provided from distinct values of gradient index when h/l = 20 in Fig. 8 are clearly observed. However, when h/l decreases and the size effect becomes more profound, those discrepancies are smaller and the results are close to each other when h/l = 1. As h/l in the range of $[10, 20]$, the displacements increase gradually and finally become stable. From that point the obtained results are comparable to those from the classical theory. The bending deformation of FG micoplates with different boundary conditions are also illustrated in Fig. 10.

4.2.2. Vibration and buckling analysis

The normalized fundamental natural frequencies and critical buckling loads of the square FG microplates with various load patterns are given in Tables 12-15. Their variations with respect to the size effect, gradient index and thickness ratio are also plotted in Figs. 9b, 9c and 11. It is seen that smaller critical buckling loads are obtained when both in-plane and shear buckling loads are considered ($N_x = N_y = N_{xy} = 1$). As expected, with the same thickness ratio, the results are seen to have largest values for a full ceramic microplate whose thickness is equal to the length scale parameter (h/l = 1). They go down when larger values of the gradient index n and the ratio of h/l are considered. In addition, the maximum and minimum results correspond to the microplates with CCCC and SFSF boundary conditions. The natural frequencies and critical buckling loads increase remarkably when the ratio h/l is relatively small ($h/l < 5$) and approaches to 1 as observed in Figs. 9b, 9c and 11. When $h/l > 5$, the results decrease gradually and turn into stable as they converge toward those produced from the classical theory. This also means that the size effect on free vibration and buckling is not considerable when h/l is relatively large, especially when $h/l > 15$ for the free vibration and $h/l > 10$ for the buckling problems. This phenomenon is in agreement with bending

response as the size effect elevates the stiffness of microplates when their sizes are comparable to the length scale parameter. Furthermore, the size effect is seen to magnify the discrepancies between the results given from different gradient indexes, thickness ratios and boundary conditions for both free vibration and buckling responses. For instance, the discrepancies between the fundamental natural frequencies of CCCC microplates (a/h = 5, $h/l = \infty$) with gradient index n = 0 and $n = \infty$ is roughly 4.0, this value increases significantly to around 16.9 when h/l = 1. This phenomenon is in contrast with that observed in the static bending analysis. It is also observed that the size effect is more pronounced for the CCCC boundary condition than other three (Fig. 9). In addition, the size effect on the buckling behaviour is more considerable than that on the free vibration response, especially for CCCC microplates. For example, with a/h = 5, h/l = 1 and n = 0, the result for normalize uniaxial buckling load is about 18.7 times greater than that obtained from the classical theory, whereas the corresponding figure for the fundamental frequency is approximately 4.4. The first two free vibration and buckling mode shapes of the square FG microplates are presented for illustration purpose in Figs. 12 and 13.

5. Conclusions

In this study, the IGA approach and the MST are employed to examine the size-dependant behaviour of FG microplates. The kinematic assumptions are based on the third-order shear deformation plate theory. The rule of mixture is adopted to describe the variations of material properties through the plate thickness. The governing equations are derived by using Hamilton's principle. The IGA approach is successfully utilized to discretize the governing equations, where NURBS basis functions are used to handle the C^2-continuity. The numerical results are presented and compared with the existing ones reported in the literature. Furthermore, parametric studies are carried out to investigate the size effect in conjunction with the influences of gradient index, shear deformation and boundary conditions on the bending, free-vibration and buckling behaviour of the rectangular and circular FG microplates. Finally, some major conclusions of the present study are drawn as follows

- The success in application of the IGA approach in this study once again proves its robustness in dealing with the plate problems, especially when a high continuity of basis function is demanded.

- The size effect leads to an increase in the stiffness of the FG plates, consequently it decreases the displacements and increases the natural frequencies and critical buckling loads of microplates.

- The size effect is most pronounced when the size of the microplates is such small that the thickness is close to the length scale parameter. The remarkable effect is captured with $h/l < 10$ for bending analysis, $h/l < 5$ for both free vibration and buckling analyses. In general, when the ratio of h/l is greater than those values, the size effect reduces gradually and becomes negligible when $h/l > 20$ for all responses.

Acknowledgements

This research study was supported by a Postgraduate Research Scholarship at La Trobe University. This financial support is gratefully acknowledged.

References

[1] Koizumi M. The concept of FGM. Ceramic Transactions, Functionally Gradient Materials 1993;34:3–10.

[2] Koizumi M. FGM activities in Japan. Composites Part B: Engineering 1997;28(1-2):1–4.

[3] Brischetto S, Carrera E. Advanced mixed theories for bending analysis of functionally graded plates. Computers & Structures 2010;88(23–24):1474–1483.

[4] Ghannadpour SAM, Ovesy HR, Nassirnia M. Buckling analysis of functionally graded plates under thermal loadings using the finite strip method. Computers & Structures 2012;108–109:93–99.

[5] Yin S, Yu T, Bui TQ, Liu P, Hirose S. Buckling and vibration extended isogeometric analysis of imperfect graded Reissner-Mindlin plates with internal defects using NURBS and level sets. Computers & Structures 2016;177:23–38.

[6] Su H, Banerjee JR. Development of dynamic stiffness method for free vibration of functionally graded Timoshenko beams. Computers & Structures 2015;147:107–116.

[7] Kennedy D, Cheng RKH, Wei S, Alcazar Arevalo FJ. Equivalent layered models for functionally graded plates. Computers & Structures 2016;174:113–121.

[8] Chu F, Wang L, Zhong Z, He J. Hermite radial basis collocation method for vibration of functionally graded plates with in-plane material inhomogeneity. Computers & Structures 2014;142:79–89.

[9] Natarajan S, Baiz PM, Ganapathi M, Kerfriden P, Bordas S. Linear free flexural vibration of cracked functionally graded plates in thermal environment. Computers & Structures 2011;89(15–16):1535–1546.

[10] Ovesy HR, Ghannadpour SAM, Nassirnia M. Post-buckling analysis of rectangular plates comprising Functionally Graded Strips in thermal environments. Computers & Structures 2015;147:209–215.

[11] Dai KY, Liu GR, Han X, Lim KM. Thermomechanical analysis of functionally graded material (FGM) plates using element-free Galerkin method. Computers & Structures 2005;83(17–18):1487–1502.

[12] Altay G, Dökmeci MC. Variational principles and vibrations of a functionally graded plate. Computers & Structures 2005;83(15–16):1340–1354.

[13] Lü C, Lim C, Chen W. Size-dependent elastic behavior of FGM ultra-thin films based on generalized refined theory. International Journal of Solids and Structures 2009;46(5):1176–1185.

[14] Shaat M, Mahmoud F, Alieldin S, Alshorbagy A. Finite element analysis of functionally graded nano-scale films. Finite Elements in Analysis and Design 2013;74:41–52.

[15] Rahaeifard M, Kahrobaiyan MH, Ahmadian MT. Sensitivity analysis of atomic force microscope cantilever made of functionally graded materials 2009;:539–544.

[16] Witvrouw A, Mehta A. The use of functionally graded poly-SiGe layers for MEMS applications. Materials Science Forum 2005;492-493:255–260.

[17] Guo X, Fang D, Li X. Measurement of deformation of pure Ni foils by speckle pattern interferometry. Mechanics in Engineering 2005;27(2):21–25.

[18] Poole W, Ashby M, Fleck N. Micro-hardness of annealed and work-hardened copper polycrystals. Scripta Materialia 1996;34(4):559–564.

[19] Chong A, Lam D. Strain gradient plasticity effect in indentation hardness of polymers. Journal of Materials Research 1999;14(10):4103–4110.

[20] Lam DCC, Yang F, Chong ACM, Wang J, Tong P. Experiments and theory in strain gradient elasticity. Journal of the Mechanics and Physics of Solids 2003;51(8):1477–1508.

[21] Mcfarland A, Colton J. Role of material microstructure in plate stiffness with relevance to microcantilever sensors. Journal of Micromechanics and Microengineering 2005;15(5):1060–1067.

[22] Liu D, He Y, Tang X, Ding H, Hu P, Cao P. Size effects in the torsion of microscale copper wires: Experiment and analysis. Scripta Materialia 2012;66(6):406–409.

[23] Toupin R. Elastic materials with couple-stresses. Archive for Rational Mechanics and Analysis 1962;11(1):385–414.

[24] Mindlin R, Tiersten H. Effects of couple-stresses in linear elasticity. Archive for Rational Mechanics and Analysis 1962;11(1):415–448.

[25] Koiter W. Couple stresses in the theory of elasticity, I and II. Proc Ned Akad Wet (B) 1964;67(1):17–44.

[26] Yang F, Chong A, Lam D, Tong P. Couple stress based strain gradient theory for elasticity. International Journal of Solids and Structures 2002;39(10):2731–2743.

[27] Mindlin R. Second gradient of strain and surface-tension in linear elasticity. International Journal of Solids and Structures 1965;1(4):417–438.

[28] Mindlin R, Eshel N. On first strain-gradient theories in linear elasticity. International Journal of Solids and Structures 1968;4(1):109–124.

[29] Altan S, Aifantis E. On the structure of the mode III crack-tip in gradient elasticity. Scripta Metallurgica et Materiala 1992;26(2):319–324.

[30] Fleck N, Hutchinson J. A phenomenological theory for strain gradient effects in plasticity. Journal of the Mechanics and Physics of Solids 1993;41(12):1825–1857.

[31] Fleck NA, Hutchinson JW. Strain gradient plasticityIn: , Advances in Applied Mechanics , vol. 33. Elsevier , 1997, p. 295–361.

[32] Fleck N, Hutchinson J. A reformulation of strain gradient plasticity. Journal of the Mechanics and Physics of Solids 2001;49(10):2245–2271.

[33] Kong S, Zhou S, Nie Z, Wang K. Static and dynamic analysis of micro beams based on strain gradient elasticity theory. International Journal of Engineering Science 2009;47(4):487–498.

[34] Wang B, Zhao J, Zhou S. A micro scale Timoshenko beam model based on strain gradient elasticity theory. European Journal of Mechanics, A/Solids 2010;29(4):591–599.

[35] Akgöz B, Civalek O. Strain gradient elasticity and modified couple stress models for buckling analysis of axially loaded micro-scaled beams. International Journal of Engineering Science 2011;49(11):1268–1280.

[36] Kahrobaiyan M, Asghari M, Ahmadian M. Strain gradient beam element. Finite Elements in Analysis and Design 2013;68:63–75.

[37] Zhang B, He Y, Liu D, Gan Z, Shen L. Non-classical Timoshenko beam element based on the strain gradient elasticity theory. Finite Elements in Analysis and Design 2014;79:22–39.

[38] Li A, Zhou S, Zhou S, Wang B. A size-dependent bilayered microbeam model based on strain gradient elasticity theory. Composite Structures 2014;108(1):259–266.

[39] Ansari R, Gholami R, Sahmani S. Study of small scale effects on the nonlinear vibration response of functionally graded Timoshenko microbeams based on the strain gradient theory. Journal of Computational and Nonlinear Dynamics 2012;7(3):031009–031009–9.

[40] Shenas AG, Malekzadeh P, Mohebpour S. Vibrational behavior of variable section functionally graded microbeams carrying microparticles in thermal environment. Thin-Walled Structures 2016;108:122–137.

[41] Wang B, Zhou S, Zhao J, Chen X. A size-dependent Kirchhoff micro-plate model based on strain gradient elasticity theory. European Journal of Mechanics, A/Solids 2011;30(4):517–524.

[42] Ashoori Movassagh A, Mahmoodi MJ. A micro-scale modeling of Kirchhoff plate based on modified strain-gradient elasticity theory. European Journal of Mechanics - A/Solids 2013;40:50–59.

[43] Sahmani S, Ansari R. On the free vibration response of functionally graded higher-order shear deformable microplates based on the strain gradient elasticity theory. Composite Structures 2013;95:430–442.

[44] Li A, Zhou S, Zhou S, Wang B. A size-dependent model for bi-layered Kirchhoff micro-plate based on strain gradient elasticity theory. Composite Structures 2014;113(1):272–280.

[45] Ansari R, Gholami R, Faghih Shojaei M, Mohammadi V, Sahmani S. Bending, buckling and free vibration analysis of size-dependent functionally graded circular/annular microplates based on the modified strain gradient elasticity theory. European Journal of Mechanics, A/Solids 2015;49:251–267.

[46] Zhang B, He Y, Liu D, Shen L, Lei J. An efficient size-dependent plate theory for bending, buckling and free vibration analyses of functionally graded microplates resting on elastic foundation. Applied Mathematical Modelling 2015;39(13):3814–3845.

[47] Zhang B, He Y, Liu D, Lei J, Shen L, Wang L. A size-dependent third-order shear deformable plate model incorporating strain gradient effects for mechanical analysis of functionally graded circular/annular microplates. Composites Part B: Engineering 2015;79:553–580.

[48] Emami AA, Alibeigloo A. Thermoelastic damping analysis of FG Mindlin microplates using strain gradient theory. Journal of Thermal Stresses 2016;39(12):1499–1522.

[49] Shenas AG, Malekzadeh P. Free vibration of functionally graded quadrilateral microplates in thermal environment. Thin-Walled Structures 2016;106:294–315.

[50] Mirsalehi M, Azhari M, Amoushahi H. Buckling and free vibration of the FGM thin microplate based on the modified strain gradient theory and the spline finite strip method. European Journal of Mechanics - A/Solids 2017;61:1–13.

[51] Hughes TJR, Cottrell JA, Bazilevs Y. Isogeometric analysis: CAD, finite elements, NURBS, exact geometry and mesh refinement. Computer Methods in Applied Mechanics and Engineering 2005;194(39–41):4135–4195.

[52] Nguyen VP, Anitescu C, Bordas SPA, Rabczuk T. Isogeometric analysis: An overview and computer implementation aspects. Mathematics and Computers in Simulation 2015;117:89–116.

[53] Beirão da Veiga L, Buffa A, Lovadina C, Martinelli M, Sangalli G. An isogeometric method for the Reissner–Mindlin plate bending problem. Computer Methods in Applied Mechanics and Engineering 2012;209–212:45–53.

[54] Thai CH, Kulasegaram S, Tran LV, Nguyen-Xuan H. Generalized shear deformation theory for functionally graded isotropic and sandwich plates based on isogeometric approach. Computers & Structures 2014;141:94–112.

[55] Kim NI, Lee J. Geometrically nonlinear isogeometric analysis of functionally graded plates based on first-order shear deformation theory considering physical neutral surface. Composite Structures 2016;153:804–814.

[56] Le-Manh T, Luu-Anh T, Lee J. Isogeometric analysis for flexural behavior of composite plates considering large deformation with small rotations. Mechanics of Advanced Materials and Structures 2016;23(3):328–336.

[57] Tran LV, Phung-Van P, Lee J, Wahab MA, Nguyen-Xuan H. Isogeometric analysis for nonlinear thermomechanical stability of functionally graded plates. Composite Structures 2016;140:655–667.

[58] Nguyen-Xuan H, Tran LV, Thai CH, Kulasegaram S, Bordas SPA. Isogeometric analysis of functionally graded plates using a refined plate theory. Composites Part B: Engineering 2014;64:222–234.

[59] Thai CH, Ferreira AJM, Carrera E, Nguyen-Xuan H. Isogeometric analysis of laminated composite and sandwich plates using a layerwise deformation theory. Composite Structures 2013;104:196–214.

[60] Valizadeh N, Natarajan S, Gonzalez-Estrada OA, Rabczuk T, Bui TQ, Bordas SPA. NURBS-based finite element analysis of functionally graded plates: Static bending, vibration, buckling and flutter. Composite Structures 2013;99:309–326.

[61] Tran LV, Thai CH, Nguyen-Xuan H. An isogeometric finite element formulation for thermal buckling analysis of functionally graded plates. Finite Elements in Analysis and Design 2013;73:65–76.

[62] Kapoor H, Kapania RK. Geometrically nonlinear NURBS isogeometric finite element analysis of laminated composite plates. Composite Structures 2012;94(12):3434–3447.

[63] Thai CH, Nguyen-Xuan H, Nguyen-Thanh N, Le TH, Nguyen-Thoi T, Rabczuk T. Static, free vibration, and buckling analysis of laminated composite Reissner–Mindlin plates using NURBS-based isogeometric approach. International Journal for Numerical Methods in Engineering 2012;91(6):571–603.

[64] Thai CH, Ferreira AJM, Bordas SPA, Rabczuk T, Nguyen-Xuan H. Isogeometric analysis of laminated composite and sandwich plates using a new inverse trigonometric shear deformation theory. European Journal of Mechanics - A/Solids 2014;43:89–108.

[65] Thai CH, Nguyen-Xuan H, Bordas SPA, Nguyen-Thanh N, Rabczuk T. Isogeometric Analysis of Laminated Composite Plates Using the Higher-Order Shear Deformation Theory. Mechanics of Advanced Materials and Structures 2015;22(6):451–469.

[66] Shojaee S, Valizadeh N, Izadpanah E, Bui T, Vu TV. Free vibration and buckling analysis of laminated composite plates using the NURBS-based isogeometric finite element method. Composite Structures 2012;94(5):1677–1693.

[67] Valizadeh N, Shojaee S, Izadpanah E, Bui T, Vu V. An isogeometric approach for free vibration and buckling analysis of laminated composite plates. in BHV Topping, (Editor), ”Proceedings of the Eighth International Conference on Engineering Computational Technology”, Civil-Comp Press, Stirlingshire, UK, Paper 44, 2012;.

[68] Yu T, Yin S, Bui TQ, Liu C, Wattanasakulpong N. Buckling isogeometric analysis of functionally graded plates under combined thermal and mechanical loads. Composite Structures 2017;162:54–69.

[69] Yin S, Yu T, Bui TQ, Zheng X, Tanaka S. In-plane material inhomogeneity of functionally graded plates: A higher-order shear deformation plate isogeometric analysis. Composites Part B: Engineering 2016;106:273–284.

[70] Yin S, Yu T, Bui TQ, Liu P, Hirose S. Buckling and vibration extended isogeometric analysis of imperfect graded Reissner-Mindlin plates with internal defects using NURBS and level sets. Computers & Structures 2016;177:23–38.

[71] Yu T, Yin S, Bui T, Xia S, Tanaka S, Hirose S. NURBS-based isogeometric analysis of buckling and free vibration problems for laminated composites plates with complicated cutouts using a new simple FSDT theory and level set method. Thin-Walled Structures 2016;101:141–156.

[72] Bhardwaj G, Singh IV, Mishra BK, Bui TQ. Numerical simulation of functionally graded cracked plates using NURBS based XIGA under different loads and boundary conditions. Composite Structures 2015;126:347–359.

[73] Yin S, Yu T, Bui TQ, Nguyen MN. Geometrically nonlinear analysis of functionally graded plates using isogeometric analysis. Engineering Computations 2015;32(2):519–558.

[74] Yu TT, Yin S, Bui TQ, Hirose S. A simple FSDT-based isogeometric analysis for geometrically nonlinear analysis of functionally graded plates. Finite Elements in Analysis and Design 2015;96:1–10.

[75] Tran LV, Ly HA, Lee J, Wahab MA, Nguyen-Xuan H. Vibration analysis of cracked FGM plates using higher-order shear deformation theory and extended isogeometric approach. International Journal of Mechanical Sciences 2015;96–97:65–78.

[76] Nguyen NT, Hui D, Lee J, Nguyen-Xuan H. An efficient computational approach for size-dependent analysis of functionally graded nanoplates. Computer Methods in Applied Mechanics and Engineering 2015;297:191–218.

[77] Nguyen HX, Nguyen TN, Abdel-Wahab M, Bordas SPA, Nguyen-Xuan H, Vo TP. A refined quasi-3d isogeometric analysis for functionally graded microplates based on the modified couple stress theory. Computer Methods in Applied Mechanics and Engineering 2017;313:904–940.

[78] Liu S, Yu T, Bui TQ, Xia S. Size-dependent analysis of homogeneous and functionally graded microplates using IGA and a non-classical kirchhoff plate theory. Composite Structures 2017;172:34–44.

[79] Reddy JN. A simple higher-order theory for laminated composite plates. Journal of Applied Mechanics 1984;51(4):745–752.

[80] Bathe KJ. Finite Element Procedures. 1 edition ed. , Prentice Hall , 1996.

[81] Piegl L, Tiller W. The NURBS Book. Monographs in Visual Communications , Berlin, Heidelberg: Springer Berlin Heidelberg , 1995.

[82] Cottrell JA, Hughes TJR, Bazilevs Y. Isogeometric Analysis: Toward Integration of CAD and FEA. 1st ed. , Wiley Publishing , 2009.

[83] Auricchio F, da Veiga LB, Buffa A, Lovadina C, Reali A, Sangalli G. A fully "locking-free" isogeometric approach for plane linear elasticity problems: A stream function formulation. Computer Methods in Applied Mechanics and Engineering 2007;197(1–4):160–172.

[84] Thai HT, Choi DH. Size-dependent functionally graded Kirchhoff and Mindlin plate models based on a modified couple stress theory. Composite Structures 2013;95:142–153.

[85] He L, Lou J, Zhang E, Wang Y, Bai Y. A size-dependent four variable refined plate model for functionally graded microplates based on modified couple stress theory. Composite Structures 2015;130:107–115.

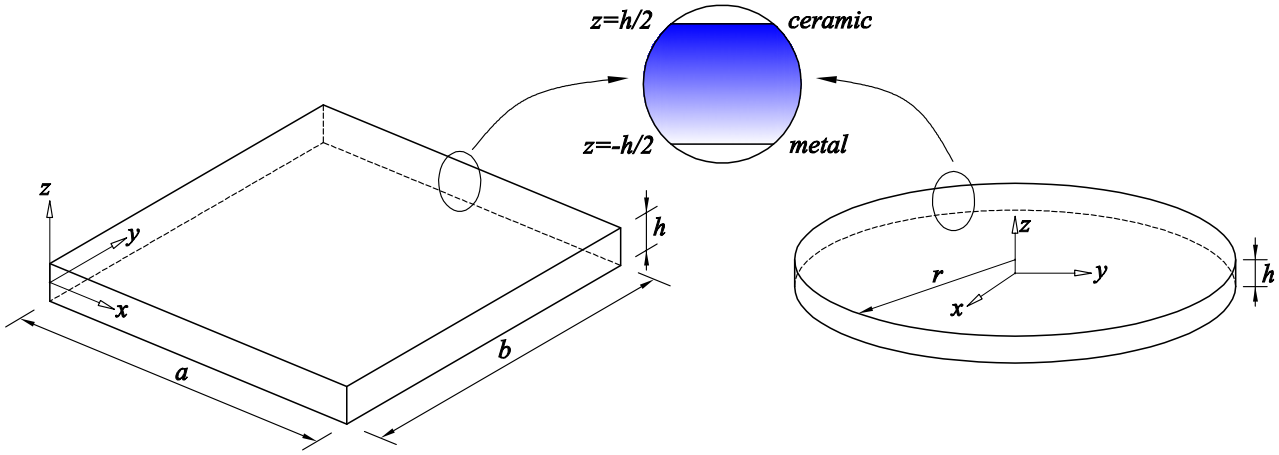

Figure 1: Configurations of rectangular and circular FG microplates

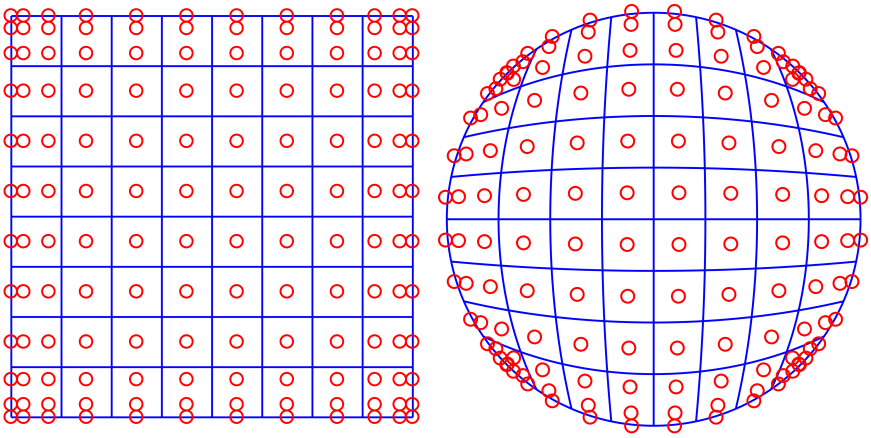

Figure 2: 8×8 meshes of square and circular plates with $p = 4$

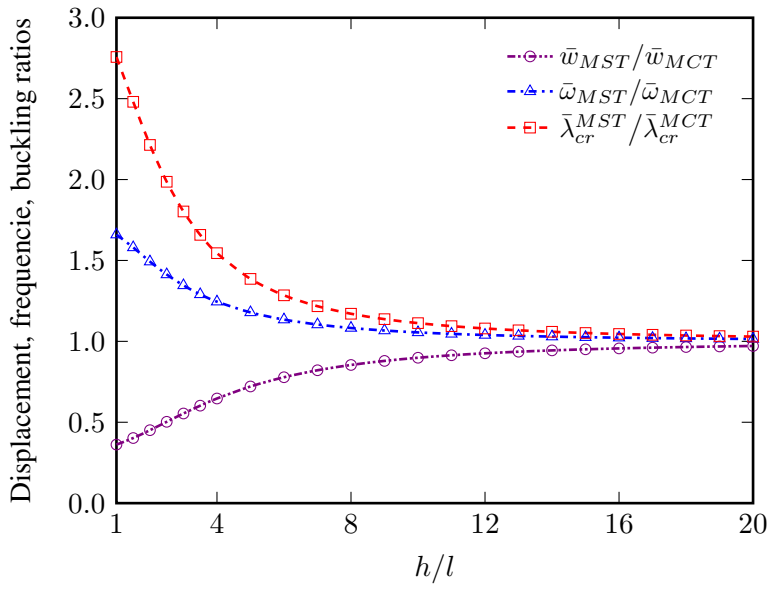

Figure 3: Comparison between effect of the MCT and MST ($a/h = 5$, $n = 2$)

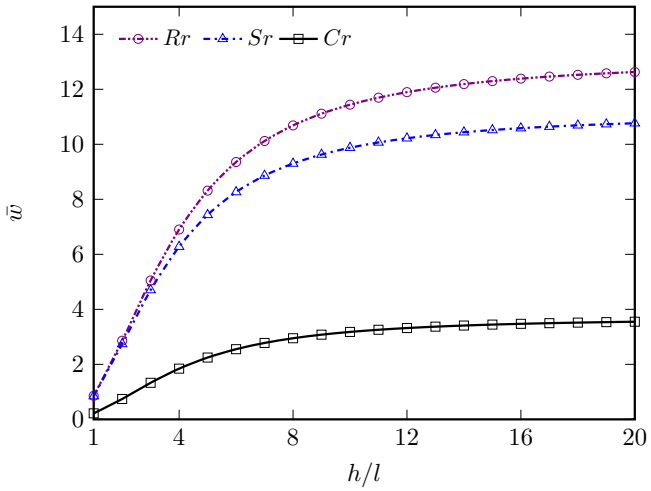

(a) Normalized displacements $\bar{w}$ under uniformly distributed load

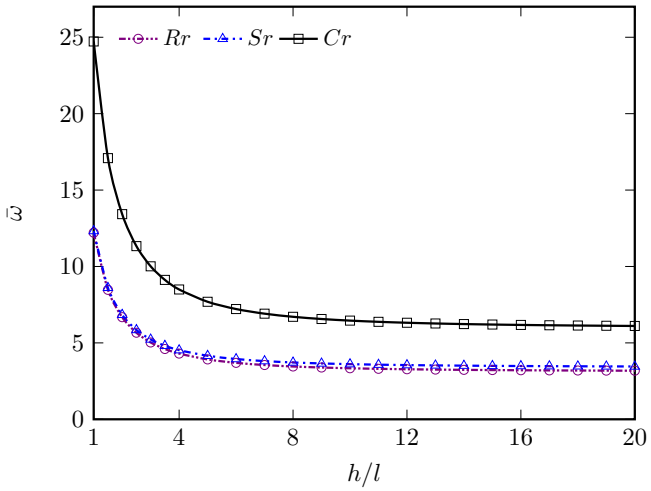

(b) Normalized fundamental frequencies $\bar{\omega}$

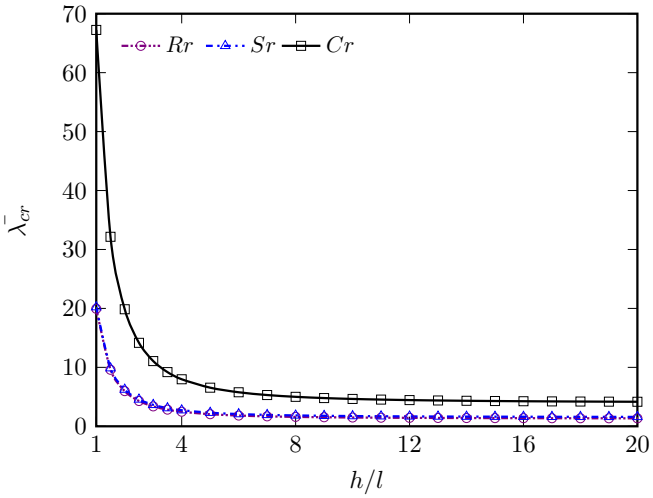

(c) Normalized critical buckling loads $\bar{\lambda}_{cr}$

Figure 4: Size effect on normalized displacements, fundamental frequencies and critical buckling loads of circular FG microplates with various boundary conditions (r/h = 5 and n = 5)

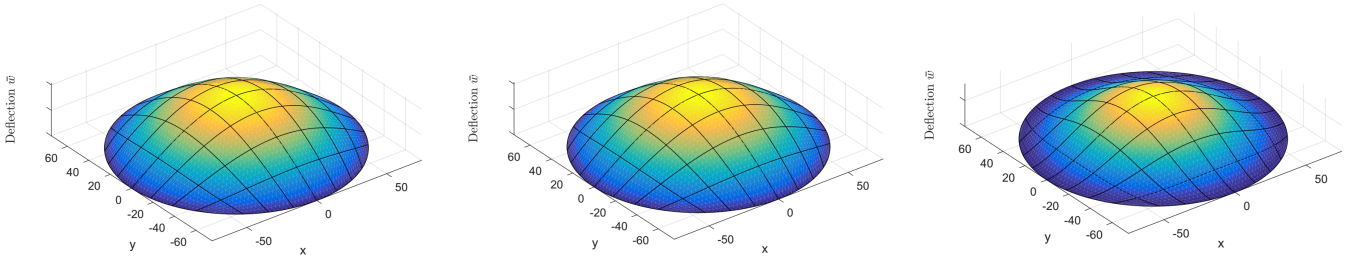

Rr Sr Cr

Figure 5: Deformed configurations of circular FG microplates

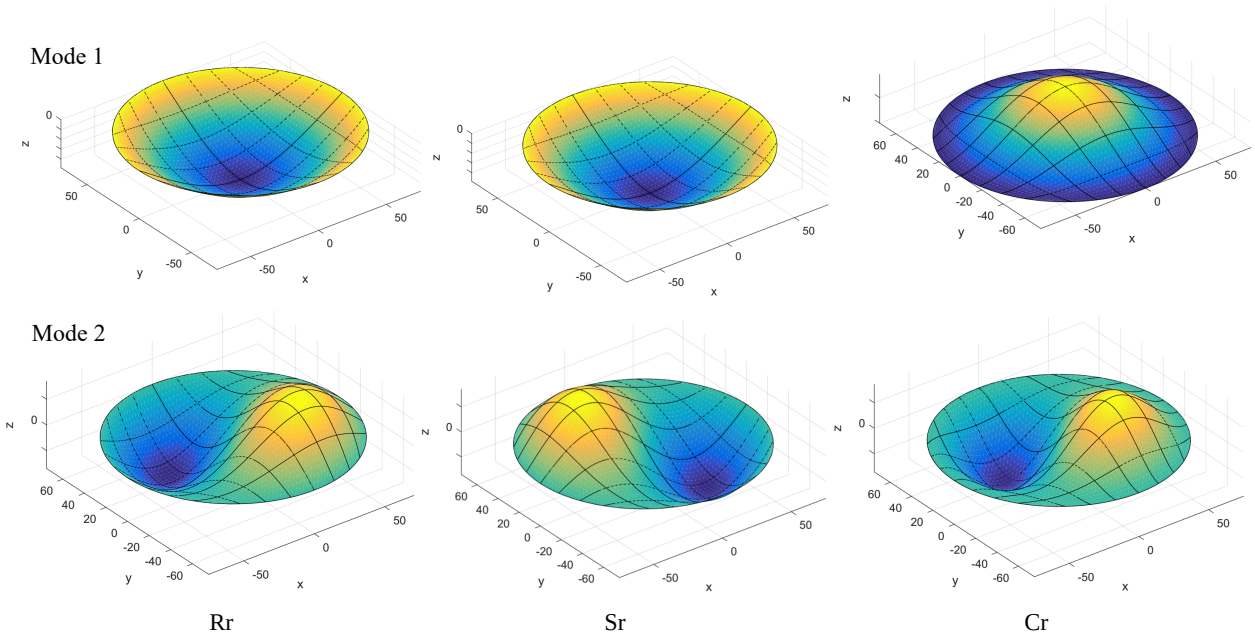

Figure 6: Configurations of vibration mode shapes of circular FG microplates

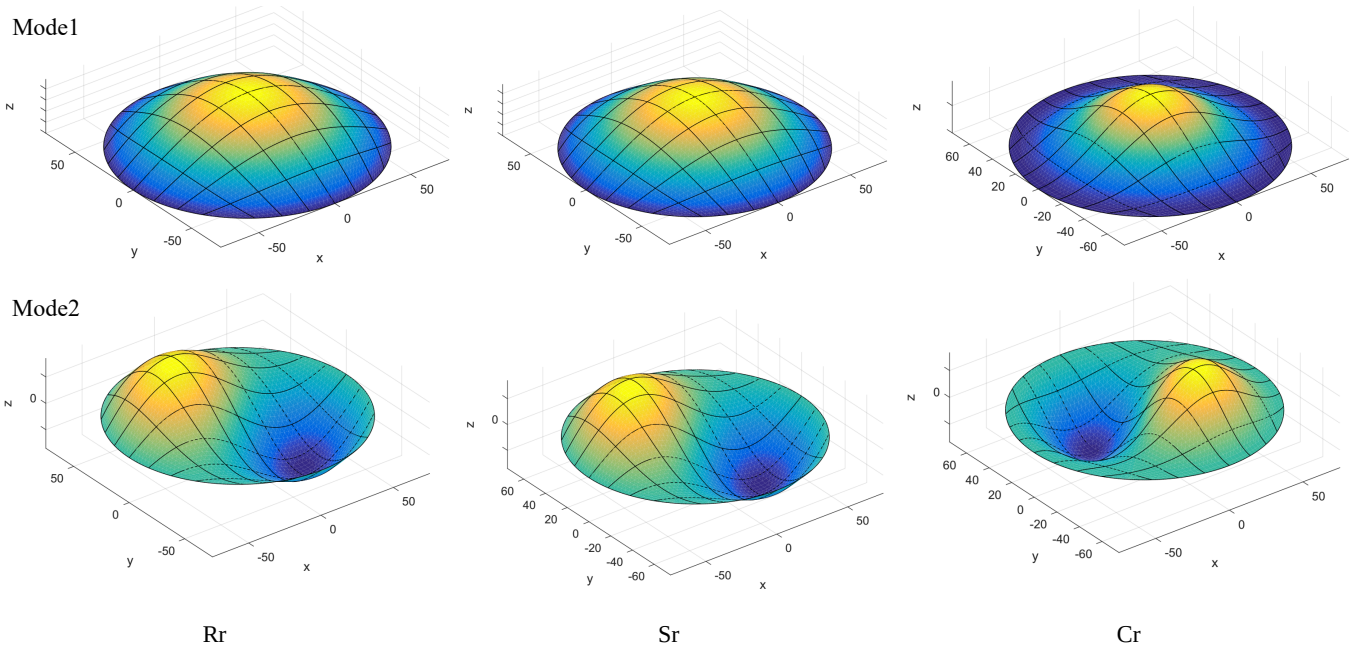

Figure 7: Configurations of buckling mode shapes of circular FG microplates

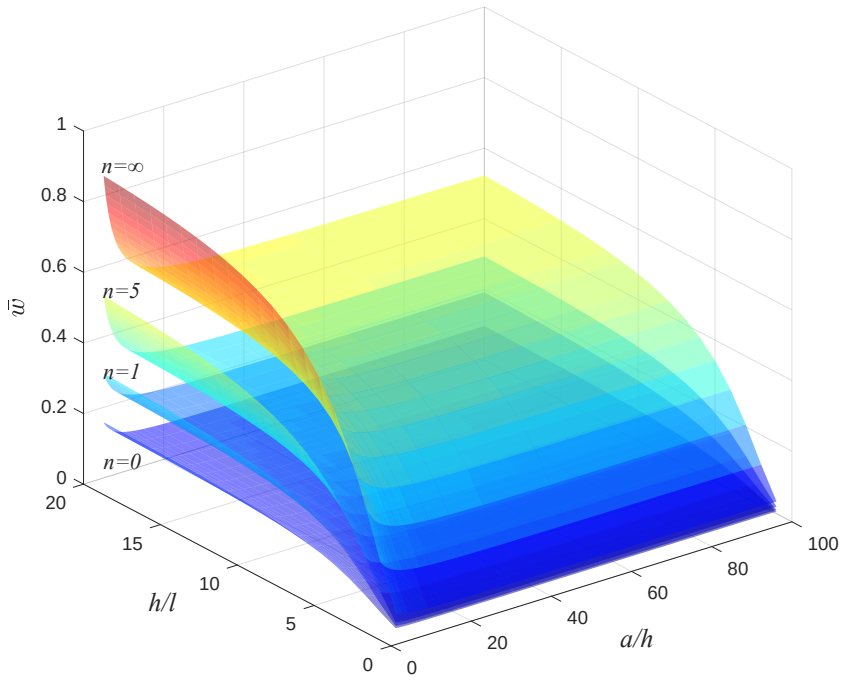

Figure 8: Variation of normalized deflection $\bar{w}$ of square CCCC FG microplate under sinusoidally distributed load with repspect to size effect (h/l), gradient index (n) and thickness ratio (a/h)

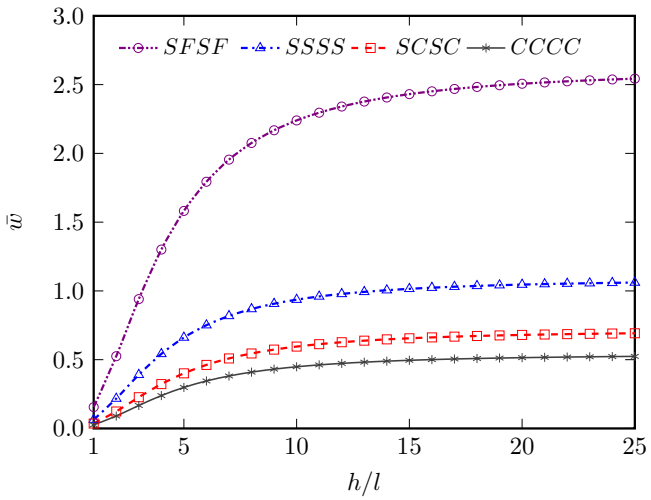

(a) Normalized displacements $\bar{w}$ under sinusoidally distributed load

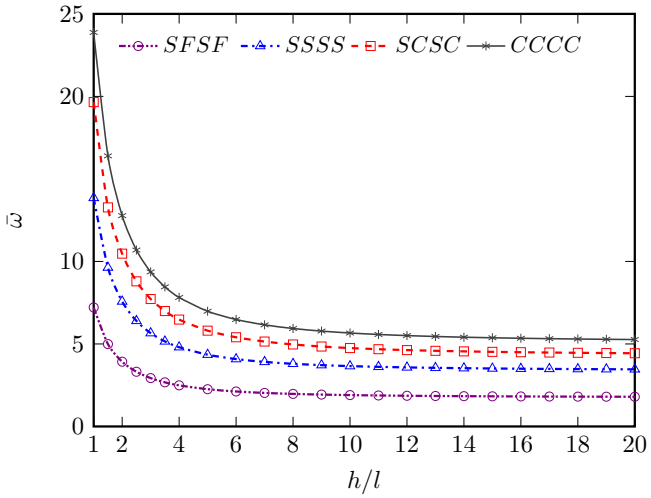

(b) Normalized fundamental frequencies $\bar{\omega}$

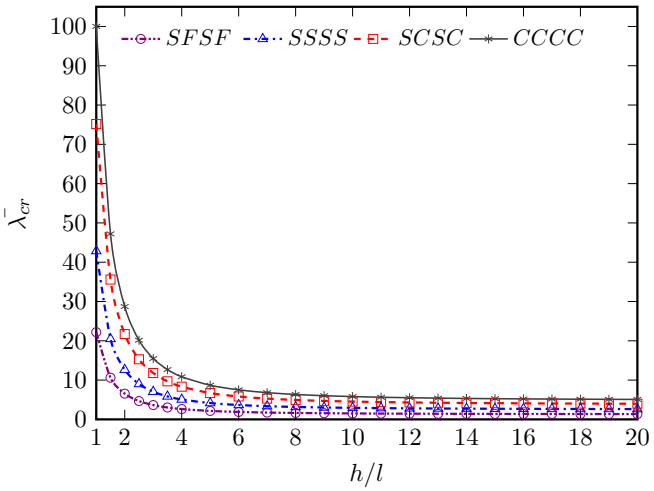

(c) Normalized critical buckling loads $\bar{\lambda}_{cr}$ ($N_x^0 = N_y^0 = 1$, $N_{xy}^0 = 0$)

Figure 9: Size effect on the normalized displacements, fundamental frequencies and critical buckling loads of square FG microplates with various boundary conditions ($a/h = 5$ and $n = 5$)

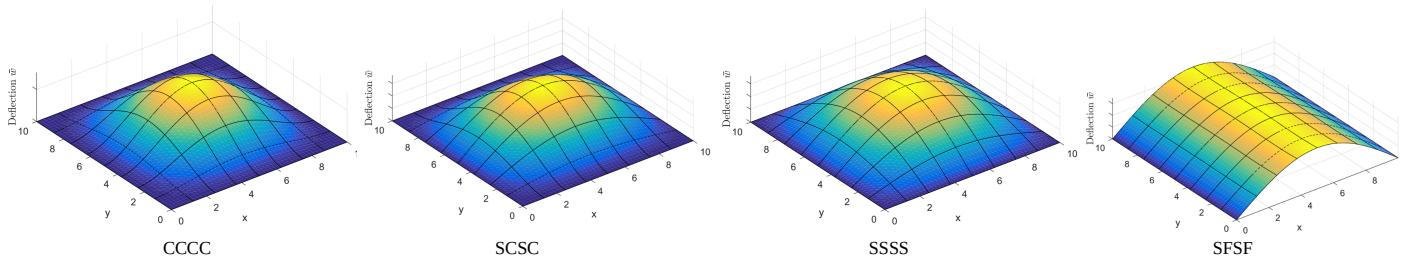

Figure 10: Deformed configurations of square FG microplates under sinusoidally distributed load

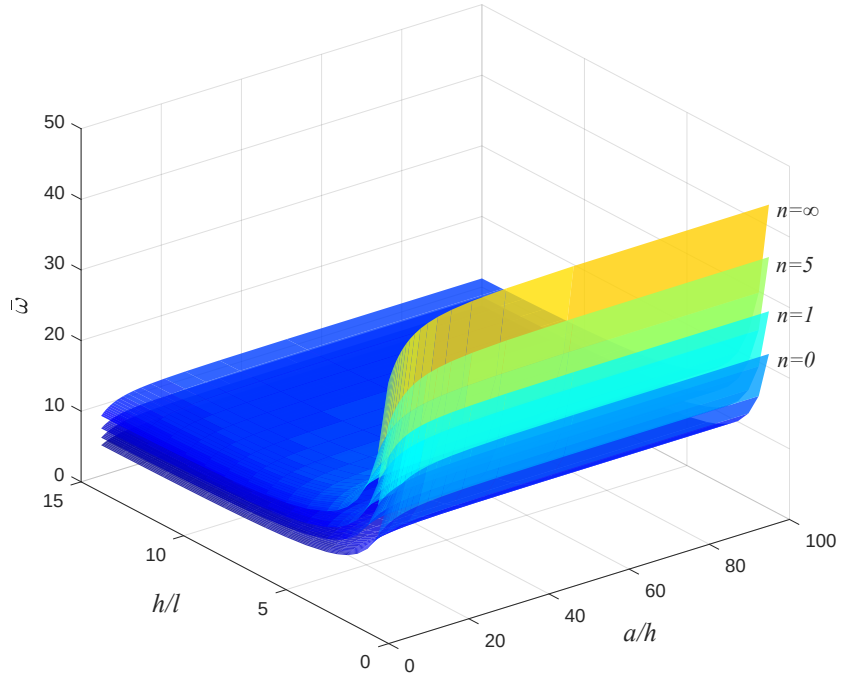

(a) Normalized fundamental frequencies $\bar{\omega}$

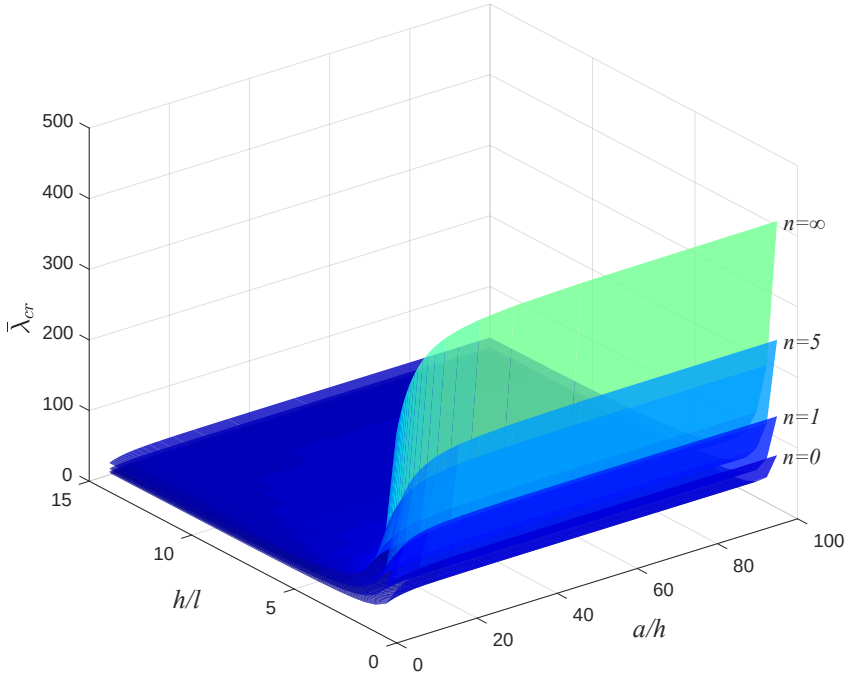

(b) Normalized buckling loads $\bar{\lambda_{cr}}$ $(N_x^0 = N_y^0 = 1, N_{xy}^0 = 0)$

Figure 11: Variation of fundamental frequencies and normalized buckling loads of square CCCC FG microplate with respect to size effect (h/l), gradient index (n) and thickness ratio (a/h)

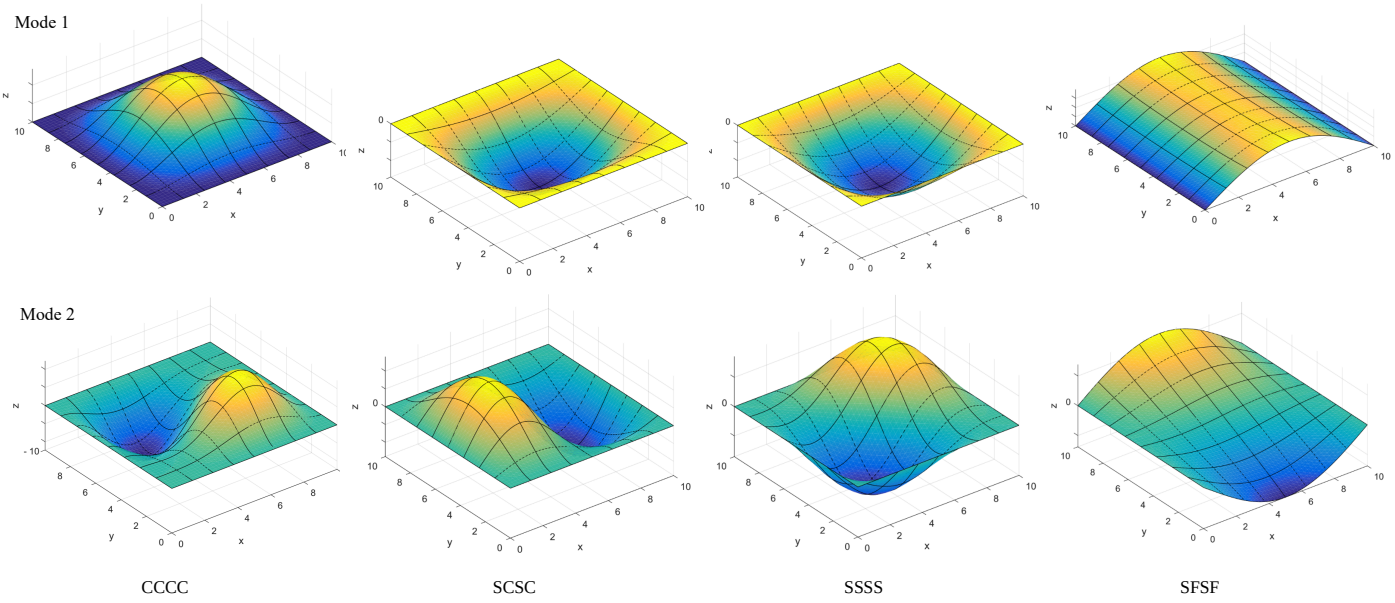

Figure 12: Configurations of vibration mode shapes of square FG microplates

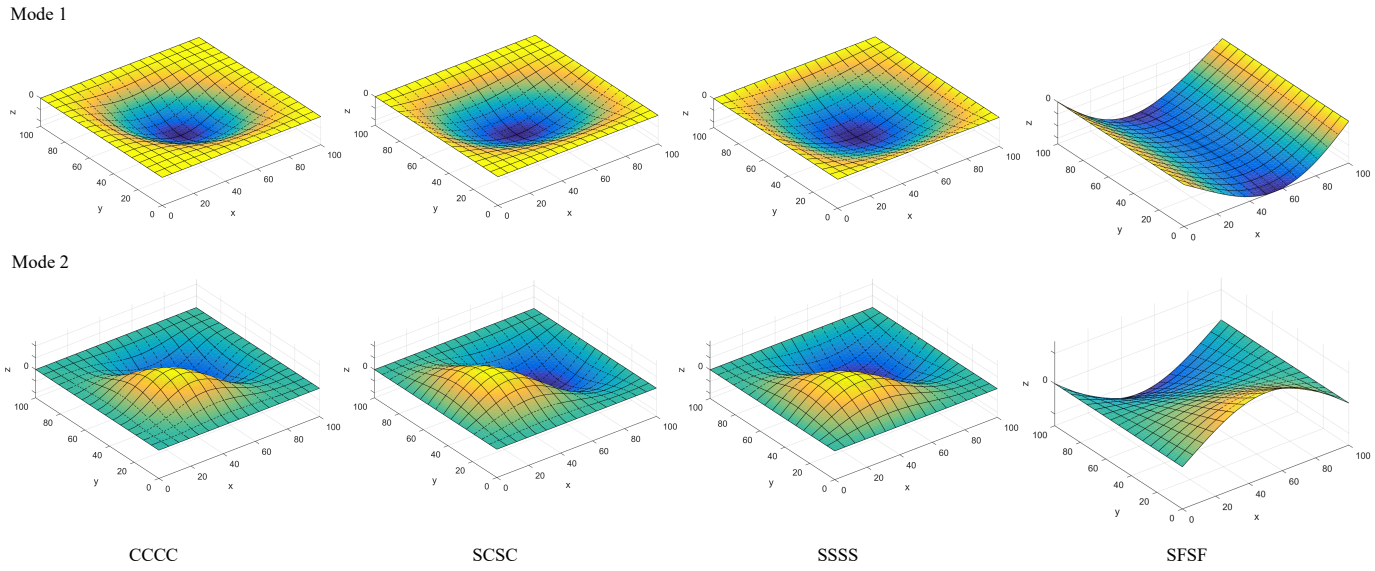

Figure 13: Configurations of buckling mode shapes of square FG microplates ($N_x^0 = N_y^0 = N_{xy}^0 = 1$)

Table 1: Midplane displacements w/h of rectangular microplates under uniformly distributed load with different mesh sizes

Boundary conditions	b/a	p-order	Mesh sizes						Ref.[50]	Ref.[42]
			2 x 2	4 x 4	8 x 8	16 x 16	64 x 64	128 x 128		
SSSS	1	3	0.0127	0.0132	0.0132	0.0132	0.0132	0.0132	0.0129	0.0127
		4	0.0133	0.0132	0.0132	0.0132	0.0132	0.0132		
	1.5	3	0.0238	0.0251	0.0249	0.0249	0.0249	0.0249	0.0245	0.0242
		4	0.0252	0.0249	0.0249	0.0249	0.0249	0.0249		
	2	3	0.0312	0.0328	0.0325	0.0325	0.0325	0.0325	0.0321	0.0318
		4	0.0330	0.0325	0.0325	0.0325	0.0325	0.0325		
CCCC	1	3	0.0022	0.0042	0.0041	0.0041	0.0041	0.0041	-	0.0040
		4	0.0043	0.0041	0.0041	0.0041	0.0041	0.0041		
	1.5	3	0.0034	0.0073	0.0070	0.0070	0.0070	0.0070	-	0.0069
		4	0.0075	0.0071	0.0070	0.0070	0.0070	0.0070		
	2	3	0.0040	0.0088	0.0080	0.0081	0.0081	0.0081	-	0.0080
		4	0.0090	0.0081	0.0081	0.0081	0.0081	0.0081		

Table 2: Comparison of normalized displacements $\bar{w}$ of square SSSS FG microplates under sinusoidally distributed load using the MCT

		n = 0		n = 1		n = 10	
a/h	h/l	Thai and Kim [84]	Present	Thai and Kim [84]	Present	Thai and Kim [84]	Present
5	∞	0.3433	0.3433	0.6688	0.6688	1.2276	1.2276
	5	0.2875	0.2875	0.5468	0.5468	1.0247	1.0247
	2.5	0.1934	0.1934	0.3535	0.3535	0.6908	0.6908
	5/3	0.1251	0.1251	0.2224	0.2224	0.4514	0.4514
	1.25	0.0838	0.0838	0.1464	0.1464	0.3052	0.3052
	1	0.0588	0.0588	0.1017	0.1017	0.2158	0.2158
20	∞	0.2842	0.2842	0.5689	0.5690	0.9538	0.9538
	5	0.2430	0.2430	0.4737	0.4737	0.8303	0.8303
	2.5	0.1693	0.1693	0.3153	0.3153	0.5986	0.5986
	5/3	0.1124	0.1124	0.2025	0.2025	0.4090	0.4090
	1.25	0.0765	0.0765	0.1349	0.1349	0.2834	0.2834
	1	0.0542	0.0542	0.0944	0.0944	0.2033	0.2033

Table 3: Comparison of normalized natural frequencies $\bar{\omega}$ of square SSSS FG microplates using the MCT

a/h	h/l	n = 0		n = 1		n = 10	
		Thai and Kim [84]	Present	Thai and Kim [84]	Present	Thai and Kim [84]	Present
5	∞	5.2813	5.2813	4.0781	4.0781	3.2514	3.2514
	5	5.7699	5.7699	4.5094	4.5094	3.5548	3.5548
	2.5	7.0330	7.0330	5.6071	5.6071	4.3200	4.3200
	5/3	8.7389	8.7389	7.0662	7.0662	5.3335	5.3335
	1.25	10.6766	10.6766	8.7058	8.7058	6.4759	6.4759
	1	12.7408	12.7408	10.4397	10.4397	7.6895	7.6895
20	∞	5.9199	5.9199	4.5228	4.5228	3.7622	3.7622
	5	6.4027	6.4027	4.9568	4.9568	4.0323	4.0323
	2.5	7.6708	7.6708	6.0756	6.0756	4.7488	4.7488
	5/3	9.4116	9.4116	7.5817	7.5817	5.7453	5.7453
	1.25	11.4108	11.4108	9.2887	9.2887	6.9013	6.9013
	1	13.5545	13.5545	11.1042	11.1043	8.1494	8.1494

Table 4: Comparison of normalized critical buckling loads $\bar{\lambda_{cr}}$ of square SSSS FG microplates using MCT

h/l	Reference	a/h = 5			a/h = 10			a/h = 20		
		n = 0	n = 1	n = 10	n = 0	n = 1	n = 10	n = 0	n = 1	n = 10
∞	He et al. [85]	15.3322	6.8611	2.7672	18.0754	7.8276	3.4969	18.9243	8.1142	3.7450
	Present	15.3322	6.8611	2.7672	18.0754	7.8276	3.4969	18.9243	8.1142	3.7450
5	He et al. [85]	18.0422	8.3399	3.3619	20.9025	9.3767	4.0513	21.7771	9.6815	4.2752
	Present	18.0422	8.3399	3.3619	20.9026	9.3767	4.0513	21.7771	9.6815	4.2752
2.5	He et al. [85]	26.1539	12.7754	5.0407	29.3735	14.0232	5.6631	30.3324	14.3832	5.8505
	Present	26.1539	12.7754	5.0407	29.3735	14.0232	5.6631	30.3324	14.3832	5.8505
5/3	He et al. [85]	39.6393	20.1658	7.7001	43.4732	21.7657	8.2906	44.5855	22.2188	8.4589
	Present	39.6393	20.1658	7.7001	43.4732	21.7657	8.2906	44.5855	22.2188	8.4589
1.25	He et al. [85]	58.4862	30.5105	11.3322	63.1958	32.6036	11.9349	64.5348	33.1882	12.1011
	Present	58.4862	30.5105	11.3322	63.1958	32.6037	11.9349	64.5348	33.1882	12.1011
1	He et al. [85]	82.6938	43.8094	15.9522	88.5416	46.5372	16.6033	90.1804	47.2914	16.7793
	Present	82.6939	43.8094	15.9523	88.5417	46.5372	16.6033	90.1804	47.2914	16.7793

Table 5: Comparison of normalized displacements $\bar{w}$ of square SSSS FG microplates under sinusoidally distributed load with $a/h = 5$

h/l	Reference	n					
		0.1	0.5	1	2	4	10
∞	Zhang et al. [46]	0.3883	0.5198	0.6688	0.8671	1.0408	1.2269
	Present	0.3785	0.5177	0.6688	0.8671	1.0409	1.2276
20	Zhang et al. [46]	0.3731	0.4983	0.6396	0.8286	0.9967	1.1790
	Present	0.3648	0.4975	0.6412	0.8307	0.9994	1.1829
10	Zhang et al. [46]	0.3341	0.4435	0.5658	0.7313	0.8843	1.0557
	Present	0.3290	0.4457	0.5709	0.7379	0.8927	1.0668
5	Zhang et al. [46]	0.2359	0.3086	0.3879	0.4980	0.6095	0.7455
	Present	0.2366	0.3153	0.3977	0.5107	0.6263	0.7678
2	Zhang et al. [46]	0.0778	0.0997	0.1223	0.1544	0.1921	0.2454
	Present	0.0803	0.1045	0.1286	0.1627	0.2034	0.2614
1	Zhang et al. [46]	0.0230	0.0293	0.0357	0.0447	0.0558	0.0724
	Present	0.0240	0.0310	0.0378	0.0475	0.0597	0.0781

Table 6: Comparison normalized natural frequencies $\bar{\omega} = \omega h \sqrt{\frac{\rho_c}{E_c}}$ of square SSSS FG microplates

a/h	Mode	h/l	Reference	n					
				0	0.5	1	2	5	10
5	1	∞	Zhang et al. [46]	0.2113	0.1804	0.1631	0.1472	0.1378	0.1358
			Present	0.2113	0.1807	0.1631	0.1472	0.1358	0.1301
		10	Zhang et al. [46]	0.2273	0.1953	0.1774	0.1603	0.1470	0.1402
			Present	0.2264	0.1948	0.1766	0.1596	0.1463	0.1394
		5	Zhang et al. [46]	0.2698	0.2344	0.2144	0.1944	0.1764	0.1666
			Present	0.2666	0.2318	0.2118	0.1920	0.1740	0.1642
		2	Zhang et al. [46]	0.4688	0.4131	0.3823	0.3490	0.3117	0.2896
			Present	0.4566	0.4032	0.3729	0.3402	0.3029	0.2807
		1	Zhang et al. [46]	0.7011	0.6290	0.5832	0.5270	0.4553	0.4150
			Present	0.8344	0.7406	0.6867	0.6266	0.5540	0.5111
	2	∞	Zhang et al. [46]	0.4623	0.3982	0.3607	0.3236	0.2918	0.2772
			Present	0.4623	0.3989	0.3607	0.3236	0.2918	0.2771
		10	Zhang et al. [46]	0.5010	0.4335	0.3945	0.3553	0.3205	0.3035
			Present	0.4978	0.4313	0.3919	0.3529	0.3181	0.3011
		5	Zhang et al. [46]	0.6019	0.5246	0.4811	0.4364	0.3939	0.3709
			Present	0.5909	0.5158	0.4724	0.4283	0.3857	0.3628
		2	Zhang et al. [46]	1.0260	0.9206	0.8536	0.7712	0.6663	0.6074
			Present	1.0255	0.9036	0.8374	0.7684	0.6914	0.6428
		1	Zhang et al. [46]	1.3904	1.2475	1.1567	1.0451	0.9029	0.8231
			Present	1.8858	1.6631	1.5460	1.4242	1.2806	1.1868
10	1	∞	Zhang et al. [46]	0.0577	0.0489	0.0442	0.0401	0.0377	0.0364
			Present	0.0577	0.0490	0.0442	0.0401	0.0377	0.0364
		10	Zhang et al. [46]	0.0619	0.0529	0.0480	0.0435	0.0405	0.0388
			Present	0.0617	0.0528	0.0478	0.0434	0.0403	0.0387
		5	Zhang et al. [46]	0.0730	0.0632	0.0578	0.0524	0.0478	0.0453
			Present	0.0725	0.0629	0.0573	0.0520	0.0474	0.0449
		2	Zhang et al. [46]	0.1258	0.1113	0.1028	0.0933	0.0825	0.0764
			Present	0.1240	0.1098	0.1013	0.0918	0.0810	0.0750
		1	Zhang et al. [46]	0.2309	0.2057	0.1907	0.1731	0.1514	0.1390
			Present	0.2268	0.2023	0.1873	0.1698	0.1482	0.1359
	2	∞	Zhang et al. [46]	0.1377	0.1171	0.1059	0.0958	0.0891	0.0857
			Present	0.1376	0.1174	0.1059	0.0958	0.0891	0.0856
		10	Zhang et al. [46]	0.1479	0.1267	0.1150	0.1041	0.0961	0.0918
			Present	0.1475	0.1266	0.1147	0.1038	0.0957	0.0915
		5	Zhang et al. [46]	0.1750	0.1518	0.1388	0.1258	0.1144	0.1082
			Present	0.1736	0.1508	0.1377	0.1247	0.1133	0.1071
		2	Zhang et al. [46]	0.3027	0.2673	0.2471	0.2250	0.2001	0.1856
			Present	0.2977	0.2632	0.2430	0.2209	0.1961	0.1818
		1	Zhang et al. [46]	0.5130	0.4603	0.4268	0.3856	0.3331	0.3037
			Present	0.5448	0.4837	0.4483	0.4090	0.3603	0.3312

Table 7: Comparison of normalized critical buckling loads $\bar{\lambda}_{cr}$ of square SSSS FG microplates

(N_x, N_y, N_{xy})	a/h	h/l	Reference	n					
				0	0.5	1	2	5	10
(1,0,0)	5	∞	Zhang et al. [46]	16.0211	10.6240	8.2245	6.3432	5.0531	4.4807
			Present	16.0211	10.6254	8.2245	6.3432	5.0531	4.4807
		10	Zhang et al. [46]	18.5456	12.4483	9.7211	7.5208	5.9295	5.2075
			Present	18.3980	12.3395	9.6338	7.4530	5.8718	5.1551
		5	Zhang et al. [46]	26.0923	17.8782	14.1785	11.0452	8.5527	7.3746
			Present	25.4873	17.4389	13.8259	10.7648	8.3136	7.1586
		2	Zhang et al. [46]	78.5650	55.3143	44.9642	35.6129	26.8501	22.4048
			Present	74.6157	52.5807	42.7188	33.7503	25.2764	21.0097
		1	Zhang et al. [46]	265.4077	188.0540	154.2099	123.1490	92.0898	75.9013
			Present	249.2773	177.1507	145.1577	115.5208	85.6764	70.2680
	10	∞	Zhang et al. [46]	18.5785	12.1213	9.3391	7.2631	6.0353	5.4528
			Present	18.5785	12.1230	9.3391	7.2631	6.0353	5.4528
		10	Zhang et al. [46]	21.3765	14.1543	10.9968	8.5479	6.9549	6.2026
			Present	21.2763	14.0850	10.9375	8.4979	6.9131	6.1674
		5	Zhang et al. [46]	29.7615	20.2387	15.9590	12.4000	9.7100	8.4445
			Present	29.3589	19.9551	15.7204	12.1985	9.5425	8.3032
		2	Zhang et al. [46]	88.3325	62.6144	50.5419	39.3331	28.9617	24.0660
			Present	85.7915	60.8187	49.0315	38.0563	27.9155	23.1847
		1	Zhang et al. [46]	297.3043	213.5682	173.7865	135.4673	97.6728	79.7717
			Present	287.0141	206.3342	167.6943	130.3251	93.4952	76.2541
(1,1,0)	5	∞	Zhang et al. [46]	8.0105	5.3120	4.1122	3.1716	2.5265	2.2403
			Present	8.0105	5.3127	4.1122	3.1716	2.5265	2.2403
		10	Zhang et al. [46]	9.2728	6.2241	4.8605	3.7604	2.9647	2.6038
			Present	9.1990	6.1697	4.8169	3.7265	2.9359	2.5775
		5	Zhang et al. [46]	13.0461	8.9391	7.0893	5.5226	4.2764	3.6873
			Present	12.7437	8.7195	6.9129	5.3824	4.1568	3.5793
		2	Zhang et al. [46]	39.2825	27.6572	22.4821	17.8064	13.4251	11.2024
			Present	37.3088	26.2909	21.3598	16.8754	12.6384	10.5051
		1	Zhang et al. [46]	132.7038	94.0273	77.1050	61.5745	46.0450	37.9506
			Present	124.6437	88.5788	72.5812	57.7620	42.8394	35.1350
	10	∞	Zhang et al. [46]	9.2893	6.0606	4.6695	3.6315	3.0177	2.7264
			Present	9.2893	6.0615	4.6696	3.6315	3.0177	2.7264
		10	Zhang et al. [46]	10.6882	7.0772	5.4984	4.2740	3.4774	3.1013
			Present	10.6381	7.0425	5.4688	4.2490	3.4565	3.0837
		5	Zhang et al. [46]	14.8807	10.1193	7.9795	6.2000	4.8550	4.2222
			Present	14.6795	9.9775	7.8602	6.0993	4.7712	4.1516
		2	Zhang et al. [46]	44.1663	31.3072	25.2710	19.6665	14.4808	12.0330
			Present	42.8958	30.4094	24.5158	19.0282	13.9578	11.5924
		1	Zhang et al. [46]	148.6522	106.7841	86.8932	67.7337	48.8364	39.8858
			Present	143.5073	103.1673	83.8473	65.1626	46.7476	38.1271

Table 8: Comparison of normalized displacements $\bar{w}$ of circular FG microplates under uniformly distributed load with $n = 1.5$

Boundary conditions	h/l	Reference	r/h				
			100	20	10	20/3	5
Rr	∞	Zhang et al. [47]	9.7669	9.7669	9.7734	9.8090	9.9266
		Present	9.5560	9.5781	9.6471	9.7621	9.9230
	10	Zhang et al. [47]	8.3050	8.3167	8.4464	8.4931	8.6275
		Present	8.1584	8.1776	8.2372	8.3364	8.4748
	5	Zhang et al. [47]	5.7673	5.7794	5.8141	5.9080	5.9775
		Present	5.6706	5.6846	5.7278	5.7993	5.8988
	2	Zhang et al. [47]	1.8370	1.8406	1.8519	1.8746	1.9019
		Present	1.8092	1.8143	1.8299	1.8557	1.8917
	1	Zhang et al. [47]	0.5349	0.5363	0.5399	0.5464	0.5556
		Present	0.5272	0.5288	0.5336	0.5417	0.5529
Sr	∞	Zhang et al. [47]	8.2119	8.2303	8.2621	8.3839	8.5551
		Present	8.0258	8.0479	8.1171	8.2325	8.3939
	10	Zhang et al. [47]	7.1440	7.1476	7.2448	7.3358	7.4543
		Present	7.0052	7.0245	7.0847	7.1847	7.3241
	5	Zhang et al. [47]	5.1735	5.1764	5.2204	5.3121	5.3811
		Present	5.0778	5.0920	5.1359	5.2085	5.3088
	2	Zhang et al. [47]	1.7693	1.7733	1.7849	1.8074	1.8359
		Present	1.7422	1.7474	1.7632	1.7892	1.8251
	1	Zhang et al. [47]	0.5289	0.5304	0.5339	0.5405	0.5497
		Present	0.5213	0.5229	0.5278	0.5358	0.5470
Cr	∞	Zhang et al. [47]	2.3765	2.3910	2.4566	2.5628	2.6947
		Present	2.3446	2.3664	2.4340	2.5459	2.7015
	20	Zhang et al. [47]	2.3378	2.2733	2.2986	2.4448	2.5724
		Present	2.2463	2.2671	2.3316	2.4378	2.5843
	10	Zhang et al. [47]	2.0226	2.0320	2.0878	2.1482	2.2749
		Present	1.9953	2.0137	2.0705	2.1632	2.2896
	5	Zhang et al. [47]	1.3785	1.3918	1.4309	1.4934	1.5768
		Present	1.3790	1.3918	1.4308	1.4934	1.5768
	2	Zhang et al. [47]	0.4381	0.4410	0.4512	0.4666	0.4877
		Present	0.4361	0.4404	0.4532	0.4733	0.4994
	1	Zhang et al. [47]	0.1270	0.1278	0.1307	0.1353	0.1415
		Present	0.1267	0.1280	0.1319	0.1378	0.1456

Table 9: Comparison of normalized natural frequencies $\bar{\omega}$ of circular FG microplates with $r/h = 5$

Boundary conditions	h/l	Reference	n					
			0	0.5	2	5	10	∞
Rr	∞	Zhang et al. [47]	4.7369	3.9449	3.0603	2.9573	2.8568	2.6787
		Present	4.7787	4.0578	3.3185	3.1228	3.0159	2.4327
	10	Zhang et al. [47]	5.1587	4.3098	3.3293	3.1333	3.1021	2.9171
		Present	5.1089	4.3697	3.5868	3.3396	3.2046	2.6008
	5	Zhang et al. [47]	6.0483	5.1568	4.0844	3.7489	3.6326	3.4202
		Present	5.9896	5.1915	4.2909	3.9174	3.7118	3.0490
	0.5	Zhang et al. [47]	10.3040	9.0789	7.5050	6.6380	6.1304	5.8270
		Present	10.2008	9.0335	7.5573	6.6810	6.1833	5.1925
	1	Zhang et al. [47]	18.8251	16.7701	14.0837	12.3157	11.3096	10.6454
		Present	18.6325	16.6167	13.9654	12.2095	11.1987	9.4844
Sr	∞	Zhang et al. [47]	4.7369	4.1906	3.8259	3.5844	3.1929	2.6787
		Present	4.7787	4.1695	3.6642	3.4042	3.1729	2.4327
	0.1	Zhang et al. [47]	5.1587	4.5444	4.0600	3.7315	3.4342	2.9171
		Present	5.1090	4.4740	3.9131	3.6086	3.3551	2.6008
	0.2	Zhang et al. [47]	6.0483	5.3535	4.7081	4.2734	3.9258	3.4202
		Present	5.9898	5.2801	4.5742	4.1573	3.8468	3.0491
	0.5	Zhang et al. [47]	10.3041	9.1899	7.8705	6.9620	6.3122	5.8270
		Present	10.2016	9.0861	7.7347	6.8400	6.2738	5.1929
	1	Zhang et al. [47]	18.8253	16.8296	14.2831	12.4965	11.4127	10.6454
		Present	18.6339	16.6500	14.0839	12.3195	11.2620	9.4851
Cr	∞	Zhang et al. [47]	9.4248	8.3094	7.4473	6.6452	6.2216	4.7938
		Present	9.2672	7.9253	6.4726	5.9806	5.7278	4.7176
	20	Zhang et al. [47]	9.5241	8.3999	7.4540	6.7594	6.2249	4.8476
		Present	9.4437	8.0898	6.6174	6.1044	5.8386	4.8075
	10	Zhang et al. [47]	10.2145	9.0188	7.9817	7.2463	6.6676	5.1991
		Present	9.9484	8.5595	7.0300	6.4559	6.1522	5.0644
	5	Zhang et al. [47]	12.0955	10.7161	9.3874	8.4811	7.7952	6.1565
		Present	11.7378	10.2094	8.4722	7.6895	7.2532	5.9752
	2	Zhang et al. [47]	20.9426	18.6309	16.0942	14.3555	13.1556	10.6597
		Present	20.1819	17.8361	15.0740	13.4247	12.4215	10.2734
	1	Zhang et al. [47]	38.8453	33.9181	29.4843	25.9336	23.9134	19.5819
		Present	36.9736	32.8279	27.9396	24.7246	22.7102	18.8209

Table 10: Comparison of normalized critical buckling loads $\bar{\lambda}_{cr}$ of circular FG microplates with $r/h = 5$

Boundary conditions	h/l	Reference	n					
			0	0.5	2	5	10	∞
Rr	∞	Zhang et al. [47]	4.0682	2.6447	1.5900	1.3242	1.1977	0.7494
		Present	4.0057	2.6114	1.5649	1.3036	1.1791	0.7416
	10	Zhang et al. [47]	4.6535	3.0700	1.8585	1.5157	1.3536	0.8572
		Present	4.5776	3.0275	1.8278	1.4906	1.3312	0.8471
	5	Zhang et al. [47]	6.3960	4.3354	2.6601	2.0871	1.8176	1.1782
		Present	6.2894	4.2716	2.6148	2.0509	1.7858	1.1630
	2	Zhang et al. [47]	18.5572	13.1386	8.2612	6.0825	5.0549	3.4185
		Present	18.2268	12.9203	8.1058	5.9649	4.9562	3.3664
	1	Zhang et al. [47]	61.9306	44.4780	28.2459	20.3445	16.6036	11.4083
		Present	60.7883	43.7009	27.6902	19.9352	16.2650	11.2233
Sr	∞	Zhang et al. [47]	4.0682	2.8094	1.9878	1.6050	1.3386	0.7494
		Present	4.0057	2.7577	1.9066	1.5470	1.3040	0.7416
	10	Zhang et al. [47]	4.6535	3.2371	2.2664	1.8051	1.4985	0.8572
		Present	4.5776	3.1741	2.1737	1.7379	1.4577	0.8471
	5	Zhang et al. [47]	6.3960	4.5008	3.0663	2.3791	1.9643	1.1782
		Present	6.2897	4.4182	2.9677	2.3054	1.9156	1.1631
	2	Zhang et al. [47]	18.5573	13.2993	8.6635	6.3794	5.2048	3.4185
		Present	18.2294	13.0654	8.4699	6.2334	5.0921	3.3671
	1	Zhang et al. [47]	61.9311	44.6359	28.6459	20.6431	16.7549	11.4083
		Present	60.7956	43.8453	28.0625	20.2114	16.4041	11.2248
Cr	∞	Zhang et al. [47]	12.6998	8.3583	5.0094	4.0408	3.6031	2.3394
		Present	12.5760	8.2987	4.9596	4.0023	3.5690	2.3274
	20	Zhang et al. [47]	13.1962	8.7174	5.2395	4.2103	3.7433	2.4309
		Present	13.0443	8.6385	5.1781	4.1620	3.7003	2.4138
	10	Zhang et al. [47]	14.6738	9.7858	5.9257	4.7156	4.1606	2.7031
		Present	14.4477	9.6557	5.8327	4.6405	4.0934	2.6729
	5	Zhang et al. [47]	20.5685	14.0342	8.6659	6.7328	5.8207	3.7889
		Present	20.0469	13.7018	8.4440	6.5500	5.6567	3.7068
	2	Zhang et al. [47]	61.6096	43.3997	27.7850	20.8056	17.3404	11.3493
		Present	59.0336	41.6855	26.6267	19.8571	16.4936	10.9074
	1	Zhang et al. [47]	207.8247	147.6316	95.9434	70.9907	58.3536	38.2835
		Present	197.9006	141.0581	91.3747	67.2458	55.0417	36.5586

Table 11: Normalized displacements $\bar{w}$ of square FG microplates under sinusoidally distributed load

Boundary conditions	a/h	l/h	n					
			0	0.5	1	2	5	10
CCCC	5	∞	0.1647	0.2429	0.3113	0.4086	0.5437	0.6304
		10	0.1404	0.2050	0.2603	0.3383	0.4476	0.5214
		5	0.0984	0.1420	0.1774	0.2267	0.2968	0.3505
		2	0.0322	0.0459	0.0559	0.0693	0.0893	0.1081
		1	0.0095	0.0135	0.0163	0.0200	0.0256	0.0313
	10	∞	0.1170	0.1773	0.2295	0.2967	0.3676	0.4121
		10	0.1016	0.1521	0.1951	0.2517	0.3161	0.3582
		5	0.0730	0.1068	0.1349	0.1733	0.2233	0.2584
		2	0.0247	0.0349	0.0430	0.0547	0.0734	0.0884
		1	0.0074	0.0103	0.0126	0.0159	0.0216	0.0265
SCSC	5	∞	0.2191	0.3248	0.4170	0.5458	0.7163	0.8251
		10	0.1875	0.2751	0.3498	0.4539	0.5951	0.6892
		5	0.1323	0.1914	0.2393	0.3058	0.4003	0.4703
		2	0.0437	0.0622	0.0758	0.0942	0.1230	0.1483
		1	0.0129	0.0183	0.0222	0.0272	0.0355	0.0432
	10	∞	0.1627	0.2472	0.3201	0.4133	0.5086	0.5685
		10	0.1415	0.2122	0.2724	0.3513	0.4389	0.4961
		5	0.1019	0.1492	0.1886	0.2425	0.3118	0.3604
		2	0.0345	0.0488	0.0602	0.0768	0.1035	0.1246
		1	0.0103	0.0144	0.0176	0.0223	0.0306	0.0375
SFSF	5	∞	0.8258	1.2567	1.6279	2.1008	2.5751	2.8740
		10	0.7174	1.0769	1.3833	1.7837	2.2214	2.5108
		5	0.5157	0.7558	0.9564	1.2306	1.5767	1.8256
		2	0.1747	0.2473	0.3058	0.3905	0.5223	0.6311
		1	0.0521	0.0731	0.0896	0.1138	0.1543	0.1895
	10	∞	0.7577	1.1645	1.5128	1.9424	2.3197	2.5585
		10	0.6590	0.9975	1.2851	1.6518	2.0189	2.2577
		5	0.4743	0.6981	0.8861	1.1408	1.4546	1.6705
		2	0.1604	0.2259	0.2801	0.3610	0.4927	0.5938
		1	0.0477	0.0662	0.0815	0.1050	0.1466	0.1800

Table 12: Normalized fundamental natural frequencies $\bar{\omega}$ of square FG microplates

Boundary conditions	a/h	l/h	n					
			0	0.5	1	2	5	10
CCCC	5	∞	8.1141	7.0401	6.3868	5.7292	5.1082	4.8214
		10	8.8366	7.6917	7.0119	6.3240	5.6618	5.3331
		5	10.6073	9.2862	8.5356	7.7664	6.9826	6.5428
		2	18.6696	16.4488	15.3041	14.1373	12.7751	11.8470
		1	34.4665	30.3942	28.3917	26.3815	23.8722	22.0463
	10	∞	9.8700	8.4405	7.6251	6.8944	6.3722	6.1039
		10	10.6027	9.1227	8.2766	7.4923	6.8823	6.5602
		5	12.5252	10.8954	9.9597	9.0367	8.2026	7.7407
		2	21.5745	19.0701	17.6422	16.0977	14.3324	13.2706
		1	39.5513	35.1215	32.6292	29.8609	26.4157	24.2754
SCSC	5	∞	6.8219	5.8981	5.3433	4.7990	4.3141	4.0884
		10	7.3999	6.4231	5.8475	5.2764	4.7509	4.4882
		5	8.8356	7.7231	7.0899	6.4464	5.8059	5.4476
		2	15.4332	13.6063	12.6446	11.6436	10.4706	9.7072
		1	28.4194	25.1206	23.4907	21.6662	19.6551	18.0765
	10	∞	8.0863	6.9031	6.2329	5.6405	5.2361	5.0254
		10	8.6772	7.4556	6.7605	6.1230	5.6429	5.3868
		5	10.2338	8.8961	8.1283	7.3744	6.7021	6.3288
		2	17.5888	15.5600	14.3915	13.1146	11.6480	10.7777
		1	32.2243	28.6567	26.6161	24.3082	21.4179	19.6645
SFSF	5	∞	2.7187	2.3157	2.0887	1.8909	1.7644	1.6982
		10	2.9223	2.5070	2.2711	2.0567	1.9012	1.8187
		5	3.4560	3.0019	2.7399	2.4830	2.2578	2.1351
		2	5.9604	5.2717	4.8665	4.4230	3.9237	3.6343
		1	10.9293	9.7143	8.9993	8.1924	7.2107	6.6291
	10	∞	2.8569	2.4238	2.1849	1.9842	1.8725	1.8101
		10	3.0673	2.6225	2.3740	2.1545	2.0092	1.9287
		5	3.6232	3.1414	2.8647	2.5973	2.3707	2.2455
		2	6.2497	5.5394	5.1089	4.6277	4.0827	3.7755
		1	11.4693	10.2397	9.4792	8.5867	7.4893	6.8635

Table 13: Normalized critical buckling loads $\bar{\lambda}_{cr}$ of square CCCC FG microplates

(N_x, N_y, N_{xy})	a/h	h/l	n					
			0	0.5	1	2	5	10
(1,0,0)	5	∞	26.5101	18.3442	14.3756	10.8698	7.8013	6.6326
		10	31.4968	21.8825	17.3413	13.2657	9.6834	8.2219
		5	46.0615	32.1454	25.8740	20.2634	15.1998	12.8606
		2	145.8547	102.1772	83.8887	67.8444	52.3865	43.7990
		1	498.4956	349.4104	289.0567	236.6911	183.8184	152.6231
	10	∞	40.8690	27.0706	20.9471	16.1682	12.9218	11.4711
		10	47.1529	31.6036	24.6676	19.0964	15.0971	13.2770
		5	65.7881	45.0313	35.6870	27.7817	21.5034	18.5512
		2	195.0743	137.6734	111.7391	88.0910	65.8642	54.7761
		1	655.4453	466.5827	381.8401	302.9154	223.8079	183.4780
(1,1,0)	5	∞	15.9619	10.8462	8.4588	6.4428	4.8346	4.1829
		10	18.5816	12.7234	10.0195	7.7033	5.8049	4.9931
		5	26.3589	18.2657	14.6224	11.4380	8.6877	7.3912
		2	80.3315	56.3416	46.2244	37.3139	28.7174	23.9520
		1	272.4994	191.3624	158.2961	129.4025	100.0113	82.7755
	10	∞	22.3312	14.7270	11.3805	8.8028	7.1165	6.3518
		10	25.6750	17.1507	13.3681	10.3593	8.2536	7.2866
		5	35.6659	24.3716	19.2892	15.0090	11.6489	10.0669
		2	105.2152	74.3343	60.2751	47.3980	35.3088	29.3375
		1	352.9918	251.8128	205.9116	162.8077	119.6213	97.9102
(1,1,1)	5	∞	12.3035	8.4536	6.6176	5.0142	3.6628	3.1327
		10	14.5856	10.0529	7.9440	6.0961	4.5159	3.8536
		5	21.1661	14.6889	11.7913	9.2371	6.9738	5.9126
		0.5	66.2774	46.3690	38.0922	30.8482	23.8268	19.9043
		1	226.5621	158.6582	131.3548	107.7182	83.7373	69.5105
	10	∞	18.7192	12.4034	9.5986	7.4069	5.9155	5.2510
		10	21.5819	14.4655	11.2920	8.7412	6.9032	6.0675
		5	30.0983	20.5910	16.3220	12.7125	9.8328	8.4754
		2	89.2116	62.8895	51.0679	40.3112	30.1618	25.0739
		1	299.6351	213.0730	174.4775	138.6101	102.5511	84.0768

Table 14: Normalized critical buckling loads $\bar{\lambda}_{cr}$ of square SCSC FG microplates

(N_x, N_y, N_{xy})	a/h	h/l	n					
			0	0.5	1	2	5	10
(1,0,0)	5	∞	21.5717	14.7224	11.5007	8.7423	6.4951	5.5973
		10	25.3472	17.4057	13.7266	10.5426	7.8893	6.7680
		5	36.2152	25.1186	20.1213	15.7304	11.9060	10.1218
		2	110.8890	77.6948	63.7041	51.4135	39.6283	33.1197
		1	376.2513	263.8099	218.0268	178.2763	138.3015	114.7792
	10	∞	31.4283	20.7870	16.0781	12.4183	9.9661	8.8672
		10	36.1976	24.2336	18.9077	14.6427	11.6057	10.2203
		5	50.3658	34.4511	27.2924	21.2445	16.4530	14.1983
		2	148.6571	104.9240	85.1205	67.0440	50.0703	41.6312
		1	498.4869	355.0073	290.3734	230.0893	169.7890	139.1741
(0,1,0)	5	∞	21.7832	14.7390	11.4787	8.7634	6.6397	5.7623
		10	25.3035	17.2555	13.5691	10.4513	7.9456	6.8560
		5	35.7047	24.6778	19.7329	15.4415	11.7725	10.0271
		2	107.6812	75.6427	62.0574	49.9806	38.2141	31.7719
		1	363.7008	256.2979	212.1304	172.8661	132.2536	108.9585
	10	∞	29.2413	19.2284	14.8461	11.5005	9.3658	8.3856
		10	33.5760	22.3746	17.4248	13.5161	10.8300	9.5845
		5	46.5446	31.7631	25.1208	19.5473	15.2059	13.1542
		2	136.8995	96.8310	78.4977	61.6092	45.6967	37.9095
		1	458.7997	328.1076	268.2901	211.5063	154.3263	126.0195
(1,1,0)	5	∞	12.4124	8.3847	6.5273	4.9870	3.7976	3.3058
		10	14.4116	9.8206	7.7207	5.9489	4.5337	3.9175
		5	20.3214	14.0459	11.2293	8.7862	6.7019	5.7108
		2	61.2602	43.0535	35.3135	28.4258	21.7214	18.0594
		1	206.9073	145.8737	120.7061	98.3027	75.1539	61.9117
	10	∞	16.5762	10.9012	8.4171	6.5200	5.3088	4.7532
		10	19.0392	12.6893	9.8829	7.6662	6.1422	5.4356
		5	26.4024	18.0212	14.2540	11.0923	8.6285	7.4639
		2	77.6930	54.9672	44.5632	34.9766	25.9432	21.5220
		1	260.4319	186.2871	152.3305	120.0884	87.6253	71.5538
(1,1,1)	5	∞	10.4869	7.1365	5.5690	4.2399	3.1701	2.7373
		10	12.3042	8.4203	6.6339	5.1037	3.8425	3.3016
		5	17.5901	12.1638	9.7399	7.6267	5.7918	4.9237
		0.5	53.9224	37.7888	31.0135	25.0260	19.1866	15.9740
		1	182.9811	128.5976	106.4445	86.9198	66.8009	55.1619
	10	∞	14.7746	9.7445	7.5305	5.8248	4.7074	4.2004
		10	16.9989	11.3526	8.8499	6.8605	5.4667	4.8245
		5	23.6330	16.1400	12.7780	9.9502	7.7235	6.6701
		2	69.7641	49.2708	39.9783	31.4566	23.3980	19.4161
		1	234.0112	166.9878	136.6609	108.0711	79.2092	64.7479

Table 15: Normalized critical buckling loads $\bar{\lambda}_{cr}$ of square SFSF FG microplates

(N_x, N_y, N_{xy})	a/h	h/l	n					
			0	0.5	1	2	5	10
(1,0,0)	5	∞	4.1774	2.7420	2.1160	1.6407	1.3425	1.2047
		10	4.8254	3.2126	2.5007	1.9402	1.5588	1.3820
		5	6.7457	4.6031	3.6368	2.8260	2.1987	1.9053
		2	20.0433	14.1729	11.4552	8.9578	6.6436	5.5264
		1	67.3534	48.1037	39.1782	30.7719	22.4888	18.4204
	10	∞	4.5250	2.9438	2.2658	1.7649	1.4785	1.3408
		10	5.2157	3.4462	2.6750	2.0810	1.7024	1.5225
		5	7.2773	4.9447	3.8952	3.0243	2.3703	2.0639
		2	21.6493	15.3728	12.3870	9.6005	7.0302	5.8347
		1	72.9085	52.5274	42.6449	33.0566	23.6587	19.2846
(0,1,0)	5	∞	7.5597	5.0193	3.8873	2.9967	2.3832	2.1127
		10	8.9919	6.0518	4.7353	3.6676	2.8828	2.5243
		5	13.0321	8.9606	7.1172	5.5407	4.2600	3.6552
		2	40.4714	28.6916	23.2510	18.2126	13.4669	11.1623
		1	137.8697	98.6063	80.3766	63.1111	46.0427	37.6807
	10	∞	8.9523	5.8565	4.5154	3.5071	2.8969	2.6114
		10	10.4415	6.9356	5.3943	4.1886	3.3863	3.0110
		5	14.7769	10.0783	7.9532	6.1698	4.7990	4.1603
		2	44.7173	31.7840	25.6274	19.8548	14.4953	12.0113
		1	151.3205	109.0330	88.5102	68.5542	48.9647	39.8979
(1,1,0)	5	∞	4.0486	2.6588	2.0521	1.5907	1.3002	1.1661
		10	4.6989	3.1303	2.4376	1.8914	1.5183	1.3451
		5	6.6085	4.5118	3.5659	2.7714	2.1546	1.8657
		2	19.7740	13.9881	11.3053	8.8367	6.5469	5.4432
		1	66.5814	47.5730	38.7359	30.3991	22.1888	18.1692
	10	∞	4.4052	2.8668	2.2068	1.7186	1.4385	1.3041
		10	5.0894	3.3642	2.6119	2.0317	1.6607	1.4846
		5	7.1252	4.8433	3.8161	2.9628	2.3205	2.0195
		2	21.2945	15.1240	12.1872	9.4445	6.9127	5.7355
		1	71.8162	51.7475	42.0090	32.5562	23.2915	18.9829
(1,1,1)	5	∞	3.7551	2.4737	1.9111	1.4792	1.1993	1.0717
		10	4.3771	2.9230	2.2788	1.7672	1.4107	1.2461
		5	6.1808	4.2249	3.3423	2.5983	2.0153	1.7422
		2	18.5591	13.1218	10.6116	8.3058	6.1635	5.1255
		1	62.5366	44.6323	36.3609	28.5868	20.9256	17.1474
	10	∞	4.1714	2.7174	2.0924	1.6287	1.3597	1.2312
		10	4.8239	3.1912	2.4784	1.9274	1.5724	1.4042
		5	6.7588	4.5959	3.6224	2.8127	2.2011	1.9144
		2	20.2068	14.3472	11.5639	8.9670	6.5680	5.4500
		1	68.1430	49.0728	39.8461	30.9053	22.1389	18.0491